agriculture

MDPI

*Review*

# Thermal Sensing for Crop Water-Status Assessment and Precision Irrigation: Methods, Scale Effects, and Decision Pathways

**Honglei Zhang and Zhong Tang ***

School of Agricultural Engineering, Jiangsu University, Zhenjiang 212013, China
* Correspondence: zht@ujs.edu.cn

**Abstract**

Efficient irrigation management requires reliable identification of when and where crop water limitations occur, followed by the conversion of diagnostic information into practical management actions. Thermal sensing provides a non-contact means of observing changes in canopy energy exchange associated with stomatal regulation and reduced transpiration. This review evaluates the use of thermal information across the complete decision pathway from crop water-status assessment to precision irrigation. It first examines the physiological and energy-balance mechanisms underlying canopy temperature responses and discusses how crop type, phenological stage, canopy structure, meteorological conditions, and concurrent stresses influence thermal signals. It then compares ground-based sensors, mobile systems, unmanned aerial vehicles, and satellite observations in terms of temporal continuity, spatial coverage, resolution, and operational constraints. Particular attention is given to radiometric calibration, canopy extraction, mixed pixels, observation timing, reference-temperature construction, and field validation. The performance and limitations of canopy-air temperature differences, the crop water stress index, energy-balance approaches, and data-driven models are subsequently assessed. Methodologically, this review synthesizes literature systematically retrieved from the Web of Science Core Collection, selecting studies that explicitly integrate thermal sensing, crop water status diagnostics, and precision irrigation applications. Evidence across the reviewed studies shows that thermal measurements can support spatially explicit water-stress diagnosis, but fixed thresholds and models developed under individual experimental conditions often exhibit limited transferability across crops, seasons, and environments. More reliable irrigation decisions therefore require the integration of thermal observations with soil moisture, weather data, crop models, and phenological information. Future research should prioritize traceable calibration procedures, dynamic irrigation thresholds, uncertain-ty-aware multimodal models, and multi-season field validation. The agronomic value of thermal sensing should ultimately be evaluated through its effects on irrigation water use, crop yield, water productivity, operational cost, and system robustness.

**Keywords:** crop water stress; thermal infrared imaging; canopy temperature; crop water stress index; precision irrigation

Check for updates

Academic Editor: Pau Marti

Received: 27 September 2026
Revised: 22 October 2026
Accepted: 22 October 2026
Published: 25 October 2026

**Copyright:** © 2026 by the authors. Licensee MDPI, Basel, Switzerland. This article is an open access article distributed under the terms and conditions of the Creative Commons Attribution (CC BY) license.

## 1. Introduction

Agricultural water constraints continue to intensify. Therefore, irrigation management must answer not only whether crops lack water, but also when, where, and how much water to supplement. Soil water content reflects root zone water storage. However, it cannot fully represent the actual water stress experienced by plants [1,2]. Leaf water

potential and stomatal conductance are closer to the physiological state of the plant. Yet, their limited sampling efficiency makes it difficult to characterise intra-field spatial variability [3–5]. Thermal infrared observations use canopy temperature as a signal. This technique can simultaneously record temporal variations and spatial distributions without physical contact with the plant. Consequently, it provides a basis for plant water status assessment and precision irrigation. The physiological basis of this method lies in the energy consumed by transpiration. When water supply is adequate and stomata are open, latent heat flux increases. As a result, leaf temperatures are typically lower than or close to air temperatures [6,7]. Conversely, water deficit induces stomatal closure and weakens transpirational cooling. More net radiation is then converted into sensible heat, causing the canopy to warm up [8]. However, canopy temperature is also altered by radiation, wind speed, air humidity, canopy structure, and observation scale. Therefore, an elevated canopy temperature cannot directly equate to an immediate need for irrigation.

Traditional methodologies for assessing water status, such as localized soil moisture probes or manual measurements of leaf water potential and stomatal conductance, are inherently point-based. They are often labor-intensive, time-consuming, and sometimes destructive, making it highly impractical to capture continuous spatiotemporal dynamics across heterogeneous fields. To overcome these limitations, thermal imaging has emerged as a non-contact, non-destructive, and rapid mapping technique. Its applications have expanded from single-leaf thermometry to crop water monitoring, irrigation scheduling, and yield assessment [9]. Unmanned aerial vehicles (UAVs) have enhanced the spatial resolution and deployment flexibility of thermal observations. They can identify field heterogeneities that point-based sensors often miss. Nevertheless, processes such as image acquisition, canopy segmentation, and the calculation of the crop water stress index (CWSI) remain mutually independent in many studies. This disconnect restricts the translation of thermal results into actionable management decisions [10]. Synthesising existing UAV research shows that the thermal infrared CWSI can characterise instantaneous water status. It also demonstrates potential for real-time irrigation scheduling. However, these technological advantages only translate into water savings if stress identification and intervention occur before irreversible damage sets in [11]. Therefore, evaluating thermal monitoring methods should go beyond merely comparing temperature retrieval accuracies. Evaluations must also examine the correspondence with plant water status and the actionability of irrigation data. Furthermore, they should assess the potential impacts on water savings and crop yield.

This paper focuses on the thermal infrared monitoring of crop water stress and its translation into precision irrigation decisions. It discusses four interrelated issues. First, it explores why and under what conditions canopy temperatures respond to water deficits. Second, it investigates how to reliably acquire thermal data and extract true canopy temperatures. Third, it examines how different thermal indicators and models can mitigate meteorological influences and express uncertainties. Finally, it outlines how diagnostic results can be formulated into irrigation thresholds, prescription maps, and feedback controls.

Literature retrieval was primarily based on the Web of Science Core Collection. Searches utilised combinations of keywords such as crop water stress, thermal infrared, canopy temperature, CWSI, evapotranspiration, UAV, and precision irrigation. Studies were included in the analysis if their titles and abstracts simultaneously involved thermal information, water status, or irrigation applications. The screened evidence was coded into four categories. These categories included physiological basis, data acquisition and processing, thermal indicators and models, and precision irrigation decisions. Review articles were utilised to outline overall research progress. Meanwhile, field trials and multi-season validations were used to compare methodological performances. Studies

lacking thermal information or having only indirect relationships with water diagnosis were excluded as core evidence. The analysis primarily examined observation targets, water supply treatments, thermal data sources, ground references, validation scales, and key error metrics. It distinguished among three types of validation. These were the correlation validation between temperature and physiological variables, the classification validation of stress levels, and the management validation of water-saving efficiencies.

Certain technologies exhibited inconsistent performances across different studies. In these cases, the reasons were analysed from the perspectives of canopy coverage, observation timing, and vapour pressure deficit (VPD). Baseline construction methods and phenological differences were also considered. Judgements of superiority or inferiority were not based on single correlation coefficients. Some results originated from the same experimental system but discussed sensors, indicators, or irrigation effects separately. These findings were categorised into corresponding sections based on their specific evidentiary purposes. This approach avoided mistaking repeated reporting of a single technology for independent validation. Methodologically, this paper is structured as a critical narrative review rather than a quantitative meta-analysis. While a statistical meta-analysis represents a high standard of evidence, the extreme heterogeneity in thermal sensor configurations, CWSI baseline algorithms, observation scales, and specific crop phenotypes across the current literature precludes a robust and unbiased statistical synthesis at this stage. Consequently, rather than generating new quantitative results from disparate datasets, this review meticulously curates representative figures from previously published studies to serve exclusively as illustrative paradigms. These visual integrations are not intended to "re-evaluate" raw data to hack new empirical claims, but rather to concretely visualize the complex physiological and physical mechanisms discussed. Ultimately, it aims to clarify the conditions under which specific conclusions hold true across different crops, spatial scales, and environmental contexts, supported by an expanded and robust body of multidisciplinary literature.

## 2. Physiological Basis of Canopy Temperature Response to Water Stress

Canopy temperature is not an independent stress trait. Instead, it is the combined result of root zone water supply, plant water transport, stomatal regulation, and near-surface energy exchange [12–14]. Only by clarifying this coupling relationship between physical and physiological processes can we rationally select observation periods, normalisation indicators, and validation variables. This section first discusses the soil–plant–atmosphere continuum and energy balance. It then explains how stomatal regulation manifests water limitations as thermal signals. Finally, it analyses the impacts of factors such as crop type, growth stage, salinity, nutrition, and disease on the temperature-water relationship.

### *2.1. Soil–Plant–Atmosphere Continuum and Energy Balance*

The soil–plant–atmosphere continuum describes the process by which water enters the root system from the soil, is transported through the xylem, and is subsequently lost via the stomata [15,16]. At the macroscopic soil-vegetation interface, the energy balance dictates that the absorbed net radiation ($R_n$) is partitioned into latent heat flux ($\lambda E$), sensible heat flux ($H$), and soil heat flux ($G$), represented as $R_n = \lambda E + H + G$ [17,18]. However, at the level of a single leaf or an isolated canopy, the energy balance is distinct. The soil heat flux is generally negligible, and the net radiation absorbed by the canopy ($R_{nc}$) is dissipated via canopy sensible heat ($H_c$), latent heat ($\lambda E_c$), and changes in canopy heat storage ($S$), formulated as $R_{nc} = \lambda E_c + H_c + S$. Under typical steady-state assumptions for thin leaves, $S$ is often considered negligible. Conversely, for dense canopies or under rapidly fluctuating, non-steady-state meteorological conditions, the heat storage term becomes a relevant factor

in modulating transient thermal responses. When transpiration is vigorous, more energy is utilised for water vaporisation, resulting in canopy cooling. Conversely, restricted transpiration causes the canopy to warm through sensible heat exchange. Therefore, thermal infrared sensors record the surface temperature modulated by the energy balance under hydraulic constraints [19,20]. They do not provide a direct surrogate for root zone water content. Increases in air temperature and incident radiation can elevate leaf temperatures even when the water supply remains constant. The effect of relative humidity is more nuanced: while lower relative humidity (higher vapour pressure deficit) initially increases evaporative demand and transpirational cooling under well-watered conditions, it can ultimately induce stomatal closure and canopy warming if the atmospheric demand exceeds the root water uptake capacity. Furthermore, leaf angle, observation scale, canopy height, and aerodynamic roughness can also alter aerodynamic resistance [21–23]. Accordingly, any judgement based on absolute temperature must be interpreted in conjunction with the microclimate and canopy structure present during observation.

Energy balance models can translate temperature information into estimates of evapotranspiration or transpiration. This conversion imbues thermal diagnostics with direct volumetric water implications. UAV-based thermal infrared and multispectral data from a high-density apple orchard were processed using a modified METRIC model. The correlation coefficient between the estimated transpiration and ground-based measurements reached 0.85. Reliable results were still obtained even when utilising data from a meteorological station located within 5 km of the orchard with a similar topography and microclimate [24]. As illustrated in Figure 1a,b, the regional-scale evapotranspiration map based on Landsat-METRIC shares a similar overall spatial pattern with the high-resolution map generated by UAS-METRIC-1. However, the UAV imagery further revealed evapotranspiration differences between rows and within localised areas of the orchard. This demonstrates that thermal infrared observations, supported by energy balance models, can facilitate scale transitions from regional overviews to fine-scale field mapping. In a small-scale bell pepper field, a two-source energy balance estimation yielded an $R^2$ of 0.73 against the soil water balance at a daily scale. This $R^2$ increased to 0.98 at a seasonal scale. Furthermore, varying the pixel size between 40 and 70 cm did not significantly alter the estimation results [21].

When utilising canopy temperature for evapotranspiration estimation, the model structure must be adapted to the crop canopy morphology. Three seasons of UAV thermal imaging in a drip-irrigated pecan orchard were combined with a modified SSEBop model. During the validation period, this approach achieved an $R^2$ of 0.90 and an RMSE of 0.24 mm/d, enabling the acquisition of monthly evapotranspiration rates [8]. For three-dimensional citrus canopies, visible light NDRI segmentation was integrated with a five-point, three-temperature model. Validated against sap flow measurements, the daily transpiration estimation yielded an $R^2$ of 0.72 and an RMSE of 0.35 mm/d [25]. The former approach focuses on regional parameter calibration, whereas the latter emphasises canopy geometric representation. This distinction underscores that converting temperature to water volume requires simultaneously matching both crop structure and observation conditions.

Scale effects can significantly influence the interpretation of thermal signals when the canopy is sparse or the field composition is complex. Ground-based and UAV thermal images were inputted into a three-temperature model to estimate maize and soybean transpiration. Validated against stable hydrogen and oxygen isotopes, the resulting $R^2$ values ranged from 0.84 to 0.88, with RMSEs of 0.099 to 0.104 mm/h. An increase in pixel size led to a mixture of soil and vegetation signatures. This resulted in overestimated canopy temperatures and slightly underestimated transpiration. Moreover, these errors became more pronounced as field heterogeneity increased [26]. This indicates that thermal

infrared data can be used for both stress identification and water volume accounting. However, it is essential to distinguish between canopy transpiration and soil evaporation, and to explicitly address mixed pixels. For irrigation purposes, energy balance methods are better suited for estimating the required water volume. Conversely, temperature or stress indices are more appropriate for identifying the locations and periods of stress. Thus, these two types of information are highly complementary.

### *2.2. Stomatal Regulation and Thermal Response*

When root zone water potential decreases or atmospheric evaporative demand increases, crops typically reduce stomatal conductance to limit water loss [27,28]. Stomatal closure simultaneously reduces transpiration and $CO_2$ diffusion. Consequently, leaf cooling weakens, and canopy temperature rises [29]. Therefore, stomatal conductance, transpiration rate, and net photosynthetic rate are crucial physiological variables for interpreting thermal signals [30,31]. However, this process is not linearly constant. Under mild stress or radiation-limited conditions, temperatures may rise before yield is compromised. Conversely, under severe stress, leaf rolling, senescence, and canopy thinning can alter the composition of thermal imagery. The sensitivity of thermal indicators and irrigation thresholds should correspond to the specific stage of stomatal response. They should not be directly determined by a single temperature anomaly [32–34].

Cross-crop evidence demonstrates that the ability of thermal indicators to reflect stomatal function varies with growth stage and canopy structure. During the cassava tuber formation stage, 29 days of continuous water deficit led to significant declines in net photosynthetic rate, stomatal conductance, and transpiration rate. Concurrently, vapour pressure deficit (VPD) and CWSI increased. The CWSI maintained strong correlations with all three physiological indicators [35]. For maize, a UAV optical-thermal imaging model spanning the entire growth cycle revealed that thermal bands contributed most significantly during the vegetative stage. In contrast, red-edge and near-infrared indices were more crucial during the reproductive stage [36]. Therefore, while thermal signals can reflect stomatal limitations, their application across varying growth stages requires simultaneous adjustments to spectral variables, canopy structural parameters, or reference baselines.

Changes in stomata and transpiration typically precede obvious yield losses. Nevertheless, discrepancies exist between crops and across different growth stages. When water supply to greenhouse sugarcane was halted, plant appearance exhibited no obvious changes. However, photosynthesis and transpiration had already declined, followed by increases in canopy temperature and thermal image grayscale [36]. Under alternate wetting and drying irrigation in rice, the Pearson correlation coefficient between CWSI and stomatal conductance reached 0.91. Yet, the treatment with a 20 cm drying depth still achieved a yield comparable to that of continuous flooding [37]. In soybeans, the midday canopy-air temperature difference during the flowering to pod-setting stages showed a strong relationship with grain yield. For every 1 °C increase in the canopy-air temperature difference, the average yield decreased by 273 to 304 kg/ha [38]. These results indicate that thermal signals should be interpreted in conjunction with the crop's sensitive growth stages and tolerable yield risks.

Thermal responses can emerge prior to yield losses. However, detecting thermal stress does not mandate immediate water supplementation. Well-watered maize and soybean plots can also experience brief thermal stress without subsequent yield reductions [39]. This phenomenon occurs because canopy temperature and evapotranspiration can operate under energy-limited conditions rather than water-limited conditions. Under low solar radiation or cloud cover, transpiration becomes constrained by available energy (radiation-limited transpiration) rather than root-zone water availability or hydraulic stomatal closure.

This radiation-driven constraint on transpirational cooling is physiologically distinct from the energy limitations governing photochemical carbon assimilation (photosynthesis). As demonstrated by Bhatti et al. [39], transient canopy temperature spikes occurring under energy-limited conditions do not reflect genuine plant hydraulic stress or soil moisture depletion, and thus do not impair final crop yields. Distinguishing this energy-limited thermal response from true hydraulic-driven stomatal closure caused by soil water deficits is critical to prevent misinterpreting transient temperature spikes as an immediate need for irrigation. Cotton trials further demonstrated that photosynthesis and stomatal conductance could differ by more than twofold under the same leaf temperature. However, the leaf-air temperature difference, combined with leaf temperature-derived VPD, explained over 79% of the physiological variance [40]. Consequently, canopy temperature should be regarded as a highly efficient proxy variable, rather than an unconditional substitute for stomatal conductance. Incorporating temperature differences, VPD, and stress duration into the diagnostic process helps mitigate the risk of mis-irrigation caused by weather fluctuations.

### *2.3. Crop, Growth Stage and Confounding Stress Effects*

Different crops exhibit variations in rooting depth, leaf morphology, stomatal sensitivity, canopy structure, and drought tolerance strategies. Moreover, the water requirements of a single crop differ significantly across the vegetative, flowering, grain-filling, and maturation stages. Consequently, identical canopy temperatures or CWSI values do not necessarily correspond to the same physiological consequences [41]. Salinity, nitrogen deficiency, heat stress, and pathogen infections can also trigger thermal anomalies through alterations in stomatal behaviour or leaf radiative properties. Under such conditions, temperature ceases to be a specific signal for water stress [42]. Establishing generalisable thermal diagnostic methods requires identifying the differences induced by crops, growth stages, cultivars, and compound stresses, all built upon the common foundation of energy balance.

Cross-cultivar and multi-temporal observations indicate that the interpretation of water status via thermal indicators is mutually influenced by stress severity and the observation window. Synchronised thermal imagery, visible light imagery, relative water content, and hyperspectral data from 10 rice genotypes demonstrated that CWSI yielded an $R^2$ of 0.63 with relative water content, effectively identifying drought tolerance rankings. A partial least squares model integrating spectral data and CWSI achieved a calibration $R^2$ of 0.94 and a cross-validation $R^2$ of 0.71 [43]. Conversely, multi-temporal observations of 10 wheat cultivars revealed that negative correlations between canopy temperature and leaf area index, photosynthesis, transpiration, stomatal conductance, and biomass were primarily evident under non-irrigated and single-irrigation treatments. These correlations weakened when the water supply was more adequate. Furthermore, the ability of temperature to differentiate drought resistance prior to grain filling was limited [44]. Thermal indicators can assist in cultivar screening. However, their application must be confined within defined ranges of stress intensity and specific growth stages.

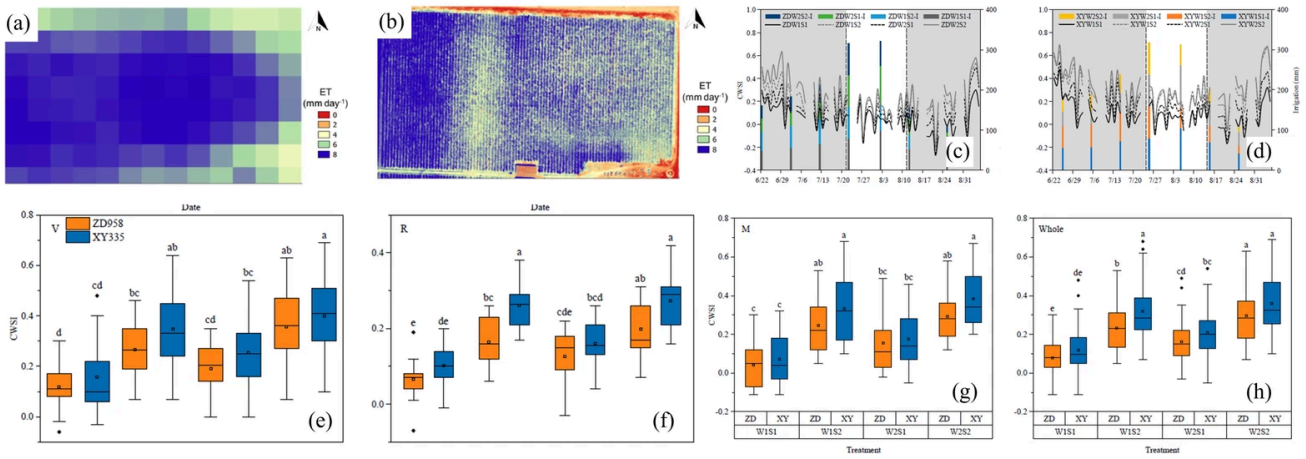



**Figure 1.** Illustrative examples visualizing the scale effects in energy balance and the confounding impacts of compound stresses on canopy thermal signals: (**a**) spatial distribution of 24 h evapotranspiration in an apple orchard based on Landsat-METRIC; (**b**) high-resolution spatial distribution of evapotranspiration based on UAS-METRIC-1 (Adapted from [24] to illustrate how fine-scale spatial heterogeneity is lost at satellite scales); (**c**,**d**) seasonal CWSI variations of two maize genotypes under different water and salt treatments; (**e**–**h**) average CWSI differences of two genotypes during the vegetative, reproductive, maturation, and entire growth stages (Adapted from [45] to visually demonstrate the 'multiple causes, single effect' phenomenon, where different stresses induce similar thermal responses). The differences in CWSI between two genotypes are analyzed by one-way ANOVA during different growth stages, respectively. Different letters denote significant differences ($p < 0.05$) by a Tukey's posthoc test for means comparison.

Compound stresses cause thermal signals to exhibit a 'multiple causes, single effect' characteristic. Determining the source of these anomalies necessitates the joint analysis of physiological and environmental variables. In wheat trials with varying water and nitrogen combinations, the simplified CWSI produced $R^2$ values of 0.73, 0.63, and 0.73 with relative water content, stomatal conductance, and transpiration, respectively. It also correlated significantly and negatively with grain yield [46]. Under combined water and salinity treatments, different maize genotypes and growth stages corresponded to distinct non-stressed baselines. Nevertheless, stage-specific CWSI could still explain variations in water potential, stomatal conductance, photosynthesis, biomass, and yield [45]. Figure 1c,d illustrate that two maize genotypes exhibited different seasonal CWSI variations under various water and salinity combinations. Figure 1e–h further demonstrate that this discrepancy persists when comparing the average CWSI across the vegetative, reproductive, maturation, and entire growth stages. This indicates that both the absolute level and the seasonal response of CWSI are simultaneously influenced by genotype, stress combinations, and phenological stages. Results from drought-heat stress trials involving 46 wheat genotypes also revealed that lower canopy temperatures and delayed flag leaf senescence frequently co-occurred with higher grain yields [47]. Therefore, thermal phenotyping is suitable for comprehensive screening. However, it struggles to independently isolate the specific effects of water deficit, salinity, and high temperatures.

Confounding stresses can induce temperature changes in the same or even opposite directions. This makes it difficult to attribute stress solely based on average canopy temperature. Grapevine regions infected by downy mildew warmed under adequate water supply, yet exhibited lower temperatures than other leaf areas under severe water deficit. Spatial deviations along pixel temperature profiles could identify infection sites at least three days before visible symptoms appeared [48]. In cotton trials combining water and NPK treatments, the correlation coefficients of CWSI with stomatal conductance and soil

water content were 0.83 and 0.88, respectively [49]. Consequently, thermal anomalies must be interpreted alongside spatial textures, spectral nutritional signals, soil data, and disease surveys. This comprehensive approach avoids misdiagnosing temperature elevations caused by diseases or nutritional deficiencies as water stress.

## 3. Thermal Infrared Data Acquisition and Processing

The reliability of thermal infrared diagnostics depends on the data acquisition and processing procedures. It does not solely rely on subsequent index calculations. Sensor accuracy, observation platforms, radiometric drift, and emissivity settings can all influence the credibility of canopy temperature. Viewing angles, shadows, and soil backgrounds also play significant roles. This chapter compares the observational capabilities of point-based sensors, ground mobile platforms, unmanned aerial vehicles (UAVs), and satellites. It discusses the necessary steps for radiometric calibration and canopy extraction. Furthermore, it analyses the impacts of observation timing, spatial scale, and ground validation on transitioning these methods from experimental plots to production fields.

### *3.1. Sensors and Observation Platforms*

The selection of a thermal infrared platform involves trade-offs. These trade-offs encompass temporal continuity, spatial coverage, resolution, cost, and operational complexity. Fixed infrared thermometers are suitable for continuously recording canopy temperature and supporting real-time control. However, their spatial representativeness is limited. Handheld or ground mobile systems operate close to the canopy and are easy to calibrate. Yet, they are constrained by sampling efficiency. UAVs can acquire centimetre- to decimetre-level imagery on demand. They are highly suitable for mapping field heterogeneity. Satellites offer large-scale coverage. Nevertheless, their revisit cycles, cloud cover, and thermal infrared pixel sizes limit their application in precision irrigation [50,51]. Therefore, an optimal platform applicable to all scenarios does not exist. Observation schemes should be determined by the decision scale and response timeframe, rather than merely pursuing higher spatial resolution.

Low-cost devices can lower the deployment threshold for thermal monitoring. However, their usability must still be validated using independent plant indicators and on-site meteorological conditions. A low-cost thermometry device was tested on olive trees under full irrigation and approximately 50% crop evapotranspiration replacement. It achieved coefficients of determination ($R^2$) of no less than 0.80 when compared with commercial thermal cameras, pre-dawn leaf water potential, and stomatal conductance. The $R^2$ for the crop water stress index (CWSI) was no less than 0.79, and the system did not require the manual acquisition of reference temperatures [52]. Figure 2a–d illustrate the device's internal sensors, control components, interface circuit board, outer casing, and field measurement scenarios. This demonstrates that low-cost thermal infrared systems have evolved from simple sensor integration into portable measurement units directly applicable for crop canopy temperature acquisition. A low-cost smartphone-attachable thermal camera was used for grapevine water assessment over 30 days. The $R^2$ values between CWSI and stem water potential, as well as stomatal conductance, were 0.61 and 0.74, respectively. However, wind conditions emerged as the primary source of error [53]. Cost reduction does not necessarily diminish practicality. Instead, on-site microclimatic variations determine the applicability boundaries of these devices.

Ground mobile systems can balance operational efficiency and canopy detail. They serve as an intermediate solution between handheld measurements and aerial platforms. A mobile thermal camera in a vineyard sampled at a speed of 5 km/h and a distance of 1.20 m from the canopy. Following multi-season and cross-region validation, the CWSI

and stomatal conductance indices predicted stem water potential with a maximum $R^2$ of 0.82 and a root mean square error (RMSE) of 0.123 MPa [54]. In protected agriculture, low-cost thermal arrays and temperature-humidity sensors continuously calculate CWSI. This setup can provide water status information for indoor cultivation [55]. The former approach has undergone quantitative cross-field validation. The latter highlights real-time deployment but possesses less performance evidence. Therefore, platform maturity should serve as a basis for selection.

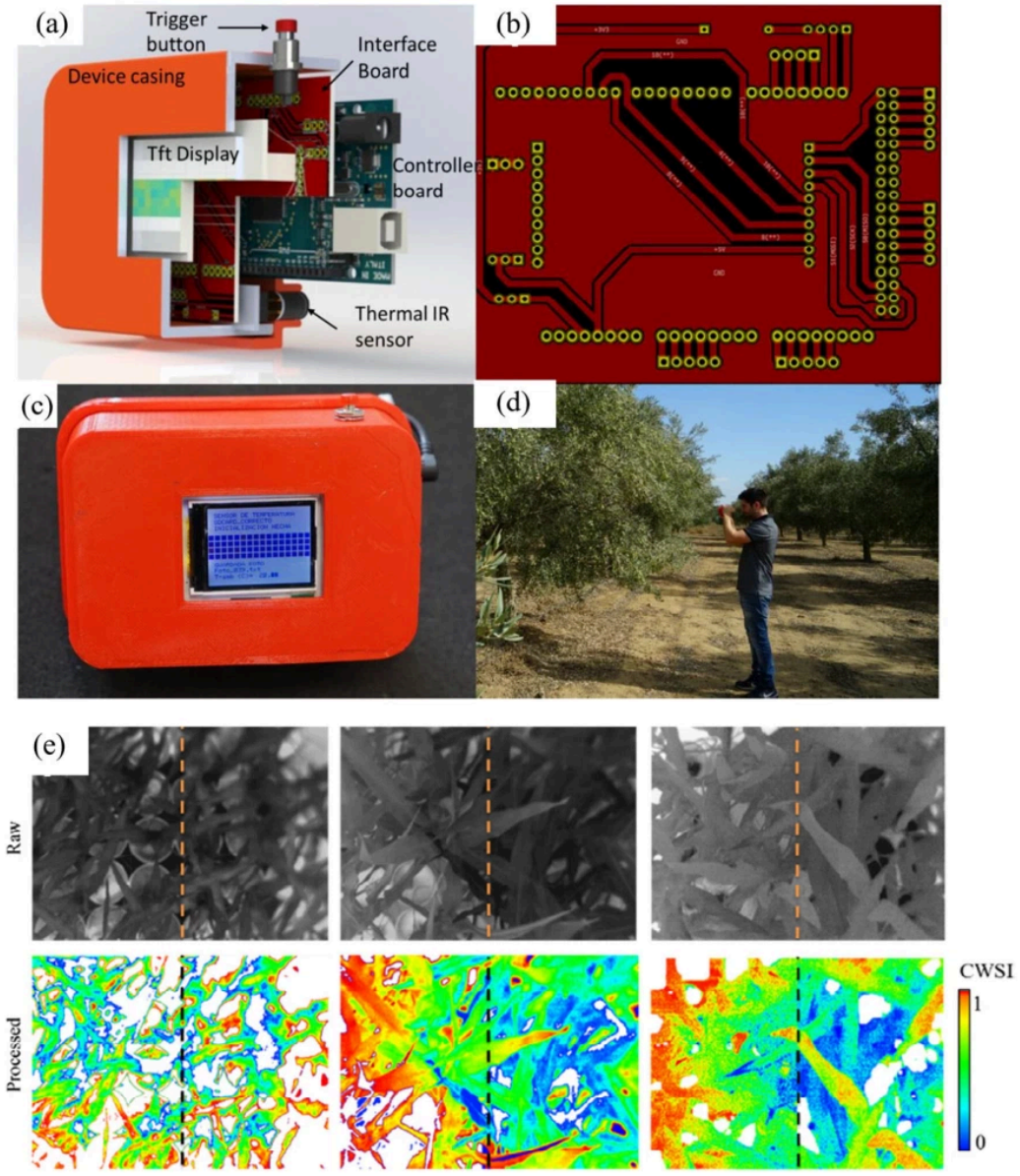



**Figure 2.** Illustrative examples demonstrating the complementarity of multi-platform thermal infrared observations regarding device morphology, temporal continuity, and spatial coverage: (**a**) internal structure of a low-cost canopy temperature measurement device for olive trees; (**b**) interface circuit board; (**c**) device casing and display interface; (**d**) field scenario of canopy temperature measurement (Adapted from [52] to visually illustrate the physical architecture of low-cost portable thermal systems); (**e**) raw thermal images, canopy processing results, and spatial CWSI distributions of greenhouse maize across different observation periods (Adapted from [56] to demonstrate the visual progression of canopy extraction and continuous stress monitoring).

The primary advantage of UAVs is the expansion of point measurements into continuous spatial phenotypic information. A commercial orchard containing five fruit tree species

was surveyed using three UAV flights in a single day. These flights were synchronised with stem water potential measurements. Differences between and within irrigation units were successfully identified. Consequently, CWSI thresholds could be established by integrating growth stages and economic risks [57]. A thermal infrared system for greenhouse maize maintained a measurement accuracy of ±0.62 °C over 80 consecutive days. The resulting CWSI explained 82% of the soil moisture variance within the 0.6 to 1.0 range [56]. Figure 2e further displays the raw thermal images, canopy processing results, and spatial CWSI distributions acquired by this system across different observation periods. Temperature differences and spatial stress patterns within the canopy can be continuously recorded across varying dates and water treatments. This highlights the advantages of fixed or near-fixed thermal imaging systems for time-series monitoring. In production management, a combined approach often balances timeliness and spatial representativeness more effectively. Such a combination might include continuous early warnings from fixed sensors, periodic mapping by UAVs, and anomaly verification via handheld devices.

### *3.2. Radiometric Calibration and Canopy Temperature Extraction*

Obtaining canopy temperature from raw thermal imagery requires resolving at least two categories of issues. First, sensor greyscale or radiance must be calibrated into comparable temperatures. Second, the target canopy must be separated from soil, shadows, branches, and weeds. Uncooled thermal cameras are prone to drift with core temperature and flight duration [58–60]. Furthermore, image stitching can introduce radiometric errors from different times into the orthomosaic [61–63]. When the canopy is sparse, a small number of high-temperature soil pixels is sufficient to elevate the average temperature [64–66]. In three-dimensional canopies, such as fruit trees and grapevines, temperature differences between sunlit and shaded leaves may also mask variations in water supply. Therefore, calibration and segmentation are crucial measurement steps ensuring that temperatures can be physiologically interpreted. They are not merely processing techniques to improve image appearance.

Calibration schemes and representative temperature statistics collectively alter the relationships between thermal indicators and physiological variables. A comparison of six UAV flights demonstrated that factory calibration and standard empirical lines resulted in a mean absolute error (MAE) of approximately 3.5 °C. This error decreased to approximately 1.5 °C when using repeated empirical lines or incorporating drift correction. The 5th percentile of canopy temperature achieved an $R^2$ of 0.85 with tree transpiration, outperforming the $R^2$ of 0.60 obtained using the mean temperature [67]. Gaussian process regression calibration combined with Gaussian mixture segmentation demonstrated higher accuracy and stability in fruit tree canopy extraction. Furthermore, the processed degrees above non-stressed (DANS) index decreased as the water supply increased [68]. Figure 3a–d intuitively compare a raw aerial thermal image with three processing outcomes. The unprocessed image contains both the target canopy and the surrounding background. Conversely, the Gaussian mixture model, Otsu binarisation, and the Otsu method combined with Gaussian blurring all exclude non-canopy regions to varying degrees. Compared to direct binarisation, pre-applying Gaussian blurring reduces the interference of local temperature fluctuations on canopy boundary extraction. This results in more continuous segmentation outcomes. Therefore, thermal imaging studies should simultaneously report reference targets, drift correction methods, flight duration, and the adopted temperature statistics.

During the canopy extraction process, the selection of temperature statistics can sometimes influence water diagnosis results more directly than the use of complex segmentation algorithms. A comparison in a 4-hectare peach orchard revealed that the RGB mask achieved the highest overall accuracy of 90%. However, when calculating CWSI using the

coldest 33% of canopy pixels, the stem water potential models derived from different segmentation methods tended to converge. Crucially, they all outperformed the whole-pixel mean [69]. For cotton and grapevine imagery, soil pixels exceeding the air temperature by 7 °C were first eliminated. Subsequently, both the histogram cold-edge method and explicit leaf segmentation successfully obtained reliable canopy temperatures [70]. After grid-fusing thermal, multispectral, and point cloud information, random forest estimations of cotton equivalent water thickness and leaf water content yielded $R^2$ values of 0.792 and 0.752, respectively [71]. Cold-edge statistics are suitable for highly efficient processing. Meanwhile, three-dimensional fusion is more advantageous for interpreting vertical canopy heterogeneity.

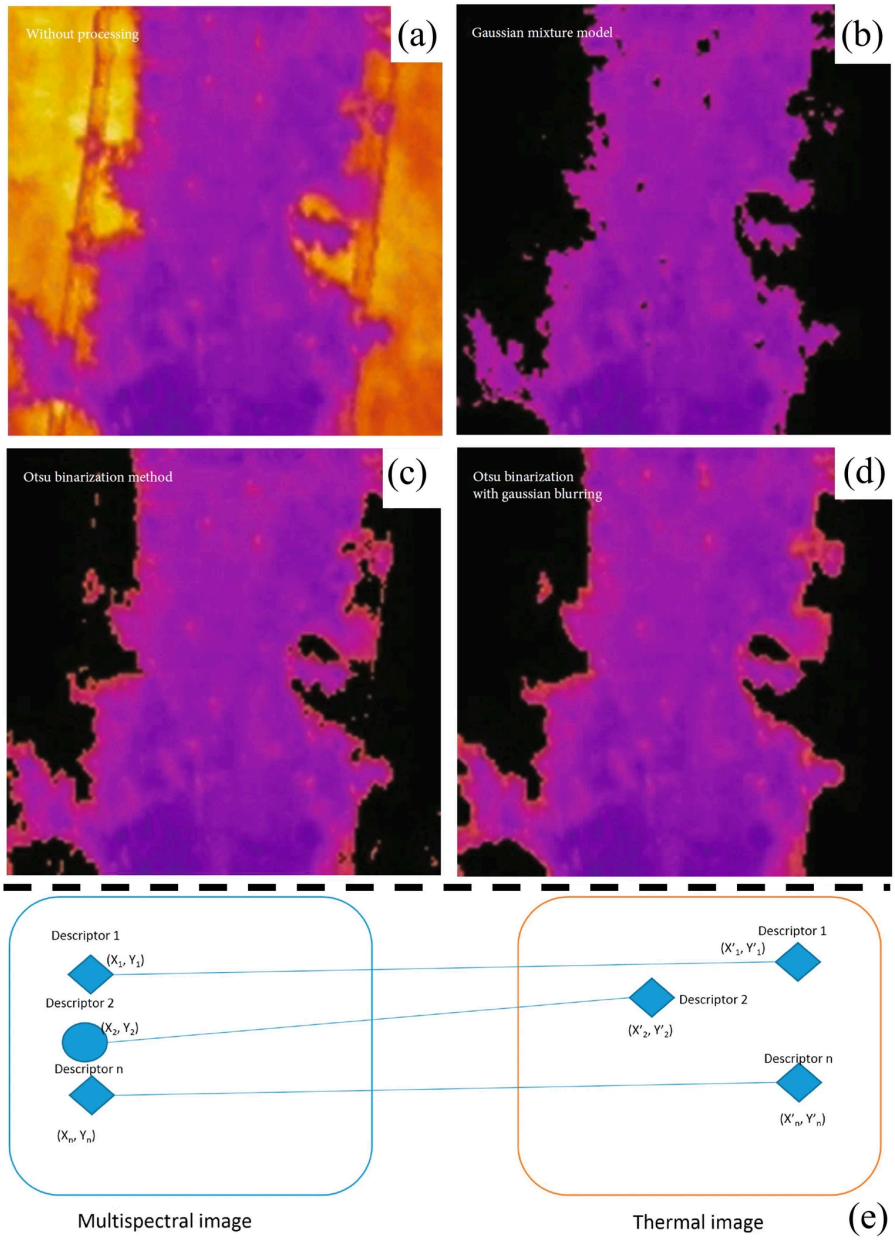



**Figure 3.** Airborne thermal infrared image processing, canopy extraction, and thermal-multispectral image coregistration workflow: (**a**) unprocessed aerial thermal image; (**b**) processing result of the Gaussian mixture model; (**c**) processing result of Otsu binarisation; (**d**) processing result of the Otsu method combined with Gaussian blurring [68]; (**e**) feature point matching between multispectral and thermal infrared images and slope-based mismatched point screening workflow [72].

Coregistering RGB or multispectral images with thermal images can effectively reduce the interference of background and shadows on canopy temperature estimation. In a vineyard, thermal and multispectral images were coregistered using modified SIFT and K-means++ algorithms, followed by the removal of shaded canopy pixels. Consequently, the $R^2$ for the relationship between CWSI and stem water potential improved from 0.64 to 0.77. The RMSE concurrently decreased from 0.2 to 0.1 MPa. The impact of shadows was particularly pronounced in drought-stressed grapevines [72]. Figure 3e summarises the key steps of this coregistration process. Initially, corresponding feature descriptor points are identified and matched between the multispectral and thermal infrared images. Subsequently, the slope distribution of the lines connecting matched points is compared. Anomalous matched points deviating from the principal direction are then eliminated. This step enhances the spatial correspondence between the two types of imagery. Thus, it provides a foundation for utilising multispectral information to identify and remove shaded pixels within thermal images. For maize imagery, 1.25 cm RGB data was utilised to assist in extracting canopy temperature from 7.8 cm thermal images. The RGRI-Otsu results achieved an $R^2$ of 0.94 and an RMSE of 0.7 °C when compared with handheld infrared thermometry [73]. This demonstrates that coregistration errors directly translate into temperature extraction errors. Therefore, it is advisable to report the number of control points, spatial residuals, and the final effective canopy proportion.

### *3.3. Observation Timing, Spatial Scale and Ground Validation*

The thermal status of crops can change rapidly within a single day. Furthermore, the spatial aggregation scale can alter the temperature distribution and its relationship with water potential. In the early morning, radiation is relatively weak. Temperature differences among treatments may not have yet formed. At midday, evaporative demand is high, and the thermal signal is typically stronger. However, high temperatures, low wind speeds, or transient cloud shadows can also disrupt energy balance assumptions. Average temperatures at the scales of individual plants, management units, and entire fields answer different management questions. A scale that is too small is susceptible to leaf posture and shadow effects. Conversely, a scale that is too large may obscure localised water deficits [74,75]. Ground validation should be synchronised with imagery in terms of time, location, and scale. It should also cover the water supply gradient as comprehensively as possible.

High spatial resolution cannot substitute for multi-temporal observations. Similarly, phenological impacts cannot be eliminated by a single ground sampling event. Results from three consecutive seasons for peach, nectarine, and flat peach indicated that the three cultivars could share a common non-water-stressed baseline and corresponding limits. However, the leaf water potential corresponding to an identical CWSI became more negative as phenology advanced. When the tree canopy area was 3 to 5 $m^2$, pixels needed to be 0.8 m or finer to achieve accurate mapping [76]. In a 7.5-hectare vineyard, imagery with sub-9 cm pixels exhibited strong relationships with synchronised stem water potential and stomatal conductance during a single observation. Nevertheless, it could not completely represent seasonal water trends. This is because other physiological processes during the maturation phase also alter canopy temperature [77]. Spatial resolution and temporal coverage should be regarded as equally important design factors.

Full-season applications require observational variables capable of adapting to changes in bare soil proportions and leaf senescence levels. A 0.25 m barley water deficit index was constructed using three periods of UAV thermal-RGB imagery. Following validation by eddy covariance, it successfully identified mature regions requiring no further irrigation during the late growth stages. This approach proved more suitable for full-season mapping

than simple surface-air temperature differences [78]. In an olive orchard subjected to five water supply treatments ranging from 30% to 125% of potential evapotranspiration, soil, stem water potential, and CWSI exhibited similar non-linear responses. There were no significant differences between empirical and analytical CWSI [79]. A comparison of four wet baselines in cotton fields further revealed that a statistical biological indicator correlated best with a theoretical wet baseline. The influence of static factors, such as sandy patches, varied throughout the season [80]. Ground validation must encompass water supply gradients and critical phenological stages. Furthermore, management zones require seasonal re-evaluation.

The choice of observation timing and reference temperature are mutually influential. Therefore, validation designs must control for both factors simultaneously. In a three-year wild blueberry trial, sampling dates significantly altered the CWSI-leaf water potential models. The biological indicator reference achieved an $R^2$ of 0.79 in 2021. In contrast, statistical references only yielded $R^2$ values between 0.34 and 0.46 across the years [81]. In cotton trials, CWSI predicted leaf water potential more stably than raw leaf temperatures. When the spatial structure of water potential was incorporated into the classification, differences among irrigation treatments became much clearer [82]. Validation should, at a minimum, record solar radiation, VPD, and wind speed. It is advisable to utilise synchronised leaf water potential or stomatal conductance alongside root zone soil moisture to form a dual reference. Furthermore, models should be tested across multiple dates.

## 4. Thermal Indicators and Models for Crop Water Stress

The common task of thermal indicators and models is to convert temperature observations, which are strongly influenced by weather, into comparable water status measurements. Simple temperature differences are easy to deploy in real time. The CWSI achieves normalisation through wet and dry references. Energy balance models provide physical constraints. Meanwhile, machine learning can integrate temperature distributions, spectra, meteorology, and soil variables. Model complexity alone does not guarantee reliability. The key lies in the sensitivity of the indicators to target physiological variables. Furthermore, the availability of reference conditions and the stability across seasons and fields are crucial. Finally, it is essential to determine whether prediction uncertainties can be correctly utilised for irrigation decisions.

### *4.1. Canopy Temperature Difference and Empirical Thresholds*

The canopy-air temperature difference, the temperature difference relative to a non-stressed canopy, and the cumulative time exceeding the crop's optimal temperature represent the most straightforward category of thermal indicators to calculate. They can be easily and continuously acquired by fixed infrared thermometers. They are also readily integrated into controllers. Their primary limitation is the inability to completely eliminate variations caused by radiation, wind, and VPD. Consequently, the same threshold is difficult to apply directly across different climates. Single-time-point indicators more closely reflect immediate stress. Conversely, integral indicators represent stress intensity and duration. Irrigation scheduling should select appropriate indicators based on the crop's tolerance to short-term temperature increases and the sampling frequency of the system.

Low-cost temperature difference indicators can be used for rapid screening. However, their thresholds require joint calibration with the year, crop type, and soil water storage conditions. In multi-level water supply trials for maize and cotton, daily and full-day stress durations increased as the irrigation volume decreased. Concurrently, the CWSI also elevated. The empirical CWSI constrained the fully watered treatment to zero and maintained values within the 0 to 1 range. This approach generally outperformed the-

oretical calculations. Nevertheless, the relationship between the maize index and yield exhibited inter-annual differences [83]. A comparison of three time-point indicators and three cumulative indicators for maize revealed the largest temperature differences among treatments during the early afternoon. DANS and DACT were highly correlated with CWSI when the threshold exceeded 28 °C. Among these, DACT required only a single canopy temperature measurement [84]. Temperature difference indicators are suitable for rapid on-site judgements. However, they do not support the direct replication of thresholds.

The dispersion degree of temperature distributions can complement mean indicators. Yet, its ability to identify mild stress is limited. When the soil water potential for sesame was at −0.1, −1.0, and −1.5 MPa, canopy temperatures under moderate and severe stress were 1.9 and 2.6 °C higher than the fully watered treatment, respectively. Various CWSI and stomatal conductance indices showed significant linear correlations with measured stomatal conductance and relative water content [85]. Following the estimation of maize canopy temperature distribution via the expectation-maximisation algorithm, the CTSD index was proposed. This indicator could respond to irrigation timing and depth. Furthermore, it correlated significantly with soil moisture deficit, leaf water potential, and stomatal conductance. However, it remained insufficiently sensitive to mild stress [86]. Distributional indicators should ideally serve as supplements to mean or baseline indicators.

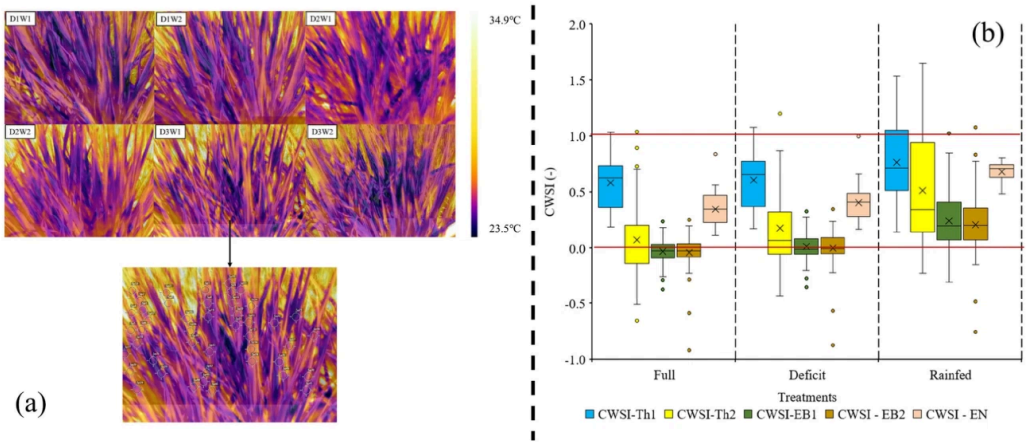



**Figure 4.** Spatial distribution of canopy temperature and expression of water stress by different CWSI reference line algorithms: (**a**) canopy thermal images and extraction results of typical canopy temperatures in rice under different drainage rates and lower soil moisture limits [87]; (**b**) distribution comparison of the theoretical CWSI, empirical baseline CWSI, and natural reference CWSI methods for maize under full irrigation, deficit irrigation, and rainfed conditions [88].

The value of simplified indicators lies in clear interpretation and low maintenance costs. They are not intended to substitute for normalisation against environmental backgrounds. During six levels of regulated deficit irrigation in sunflower, both CWSI and DANS responded to irrigation timing, irrigation depth, and root-zone water deficit. They were also closely correlated with leaf area index, intercepted photosynthetically active radiation, leaf water potential, and root growth. DANS demonstrated scheduling potential in arid and semi-arid regions [89]. A comparison of cumulative temperature distributions in rice showed that a sensitive CWSI, obtained after removing low-temperature pixels, had a better relationship with photosynthetic activity. Moreover, it could provide optimal leaf water use efficiency intervals for different growth stages [87]. Figure 4a displays the infrared images of rice under varying drainage rates and lower soil moisture limits, alongside the process of extracting canopy temperature from typical images. This intuitively reflects the spatial differences in canopy temperature caused by changing water conditions. It also illustrates that canopy temperature distribution forms an important data foundation for

constructing a sensitive CWSI. Empirical thresholds must simultaneously consider both temperature distributions and phenological information.

### *4.2. Crop Water Stress Index and Reference-Line Construction*

The CWSI normalises actual canopy temperature between states of potential full transpiration and zero transpiration using wet and dry references. It remains the most widely used thermal indicator for water status. The empirical method typically constructs a non-water-stressed baseline. It achieves this through the regression relationship between the canopy-air temperature difference of a well-watered canopy and the vapour pressure deficit (VPD) [90,91]. The theoretical method calculates upper and lower limits based on the energy balance [92]. Meanwhile, artificial reference surfaces and image statistical methods can reduce reliance on specifically treated control plots [93]. Errors in wet references, dry references, or meteorological inputs can alter the zero point and scale of the index. Therefore, the CWSI reference line should be regarded as a model component requiring thorough validation.

Different algorithms and phenological conditions can alter the scale of the CWSI. Consequently, irrigation trigger thresholds cannot be directly transferred between different methods. Six calculation algorithms were applied to fully irrigated, deficit-irrigated, and rainfed maize. These algorithms exhibited inconsistencies regarding inter-daily variations and sensitivity to soil water depletion. When root-zone water consumption exceeded 80%, the theoretical and empirical baseline methods achieved an $R^2$ of approximately 0.61 to 0.80 with the deficit in the 1.8 to 2.1 m soil layer [88]. Figure 4b further compares the distributions of the theoretical CWSI, empirical baseline CWSI, and natural reference CWSI under full irrigation, deficit irrigation, and rainfed conditions. Different methods still exhibited distinct numerical ranges under the same water supply scenario. Furthermore, the degree of dispersion in the rainfed treatment was typically greater. This indicates that the absolute value of the CWSI depends not only on crop water status but is also influenced by the reference line construction method and energy balance assumptions. Three consecutive years of citrus observations also showed that flushing and inter-annual crop load altered the non-water-stressed baseline. This occurred despite the CWSI maintaining a significant relationship with stem water potential, yielding $R^2$ values between 0.59 and 0.66 [94]. Both crop phenology and the computational pathway alter the index scale. Thus, threshold calibration must be completed separately for each.

Fixed sensors and data models can provide reference temperatures that vary with the season. However, model extrapolations must still be constrained. The non-stressed baseline of a super-high-density olive orchard exhibited seasonal differences. These differences could be partially explained by the solar elevation angle. The CWSI demonstrated the tightest relationship with maximum stomatal conductance [95]. Continuous monitoring of sugarcane revealed that stress peaked at 10:00 and 14:00. The daily CWSI reached its minimum on the second day post-irrigation. This resulted in an identified trigger range of 0.4 to 0.5 [96]. Air temperature and relative humidity were used to predict the fully watered canopy temperature of Indian mustard. The Kohonen self-organising map achieved a validation $R^2$ of 0.978. This outperformed both multiple linear regression and feed-forward neural networks [97]. Digitised wet references can reduce the need for dedicated control plots. Nevertheless, anomalous weather or unrepresented phenological stages can still cause extrapolation biases.

Artificial references improve the operational feasibility of on-site CWSI calculations. However, their materials and geometries must closely simulate the radiative and heat exchange characteristics of true leaves. Three green-tinted, hemispherical cellulose reference surfaces were used for real-time wet and dry end measurements in maize. A specific

RGB colour performed best. The dry end could be read directly, while the wet end still required conversion based on solar radiation [98]. Under various weather conditions and tree species, the surface temperature of green paper exhibited a linear relationship with the wet and dry reference leaf temperatures. Illumination significantly affected this relationship. A new CWSI relying solely on leaf temperature and the wet reference was the least sensitive to wet-end errors. Conversely, it was the most sensitive to actual leaf temperature [99]. In engineering applications, radiation, wetting state, and material ageing must be synchronously recorded. Furthermore, they should be verified against the true canopy within the season.

### *4.3. Data-Driven Models, Transferability and Uncertainty*

Machine learning can integrate non-linear relationships among temperature, spectra, structure, meteorology, and soil variables. It is well-suited for estimating stomatal conductance, water content, or CWSI from high-dimensional UAV data. However, high accuracy within a training set does not equate to transferability. If training and testing samples originate from the same season, the same field, or adjacent plots, the model may simply learn cultivar, soil background, and flight date characteristics. It might fail to learn stable water deficit mechanisms. Model evaluations should utilise independent years or locations for testing. They should also explain variable contributions and decompose errors across different stress levels and spatial scales. Furthermore, they must identify samples falling outside the training range. Physical constraints and physiological variables can provide clearer extrapolation boundaries for data-driven models.

Multi-modal fusion can alleviate the reliance of single thermal signals on phenology. However, the effective variables differ across various stages. Independent-year tests covering six key growth stages over two years for winter wheat were conducted. Thermal indicators exhibited the strongest relationship with normalised stomatal conductance and available water content during early stages. During later stages, RVI, MSR, and NDVI played more prominent roles. After variable fusion, the gradient boosting decision tree (GBDT) predicted stomatal conductance at flowering with an $R^2$ of 0.88. It predicted available water content during grain filling with an $R^2$ of 0.90 [100]. Another multi-algorithm comparison revealed that thermal bands performed best when inputted into a random forest alongside selected vegetation indices. The seasonal model achieved an $R^2$ of 0.87, whilst the post-heading model reached 0.93. SHapley Additive exPlanations (SHAP) identified RNV, thermal bands, and GRVI as the primary variables [101]. Fusion strategies must be adjusted according to the growth stage.

Deep learning can utilise the spatial features of thermal maps for stress grading. Nonetheless, category boundaries and background processing still influence its management value. A convolutional neural network (CNN) was used to identify rice under 100%, 90%, and 80% irrigation scenarios. It incorporated background temperature as a feature to adapt to variations in leaf temperature relative to air temperature [102]. As shown in Figure 5a, this method separately extracts convolutional features from the foreground canopy and background thermal images. It then applies late fusion to the high-level features of both branches. Finally, it outputs the water stress discrimination result via a Sigmoid function. Figure 5b further illustrates the classification structure after the fused features enter a multilayer perceptron (MLP). The network passes through hidden layers containing 1024, 512, and 256 neurons. It classifies the samples into fully watered, mild stress, and moderate stress categories. This structure demonstrates that background temperature is not a simple interference factor. When the difference between leaf and air temperature changes with weather, the background branch can provide an auxiliary reference for stress classification. InceptionResNet-v2 transfer learning was applied to sugarcane across 25%,

50%, and 100% available water levels. Compared to manual interpretation, its accuracy improved by 23%, 17%, and 14%, respectively [103]. Wheat hyperspectral vegetation indices were fused with canopy temperature parameters. The random forest achieved an overall accuracy of 89.47% and a Kappa of 0.85, significantly outperforming single-variable models [104]. Multi-modal and transfer learning assist in automatic grading. Nevertheless, independent regional testing and the identification of uncertain samples remain necessary.

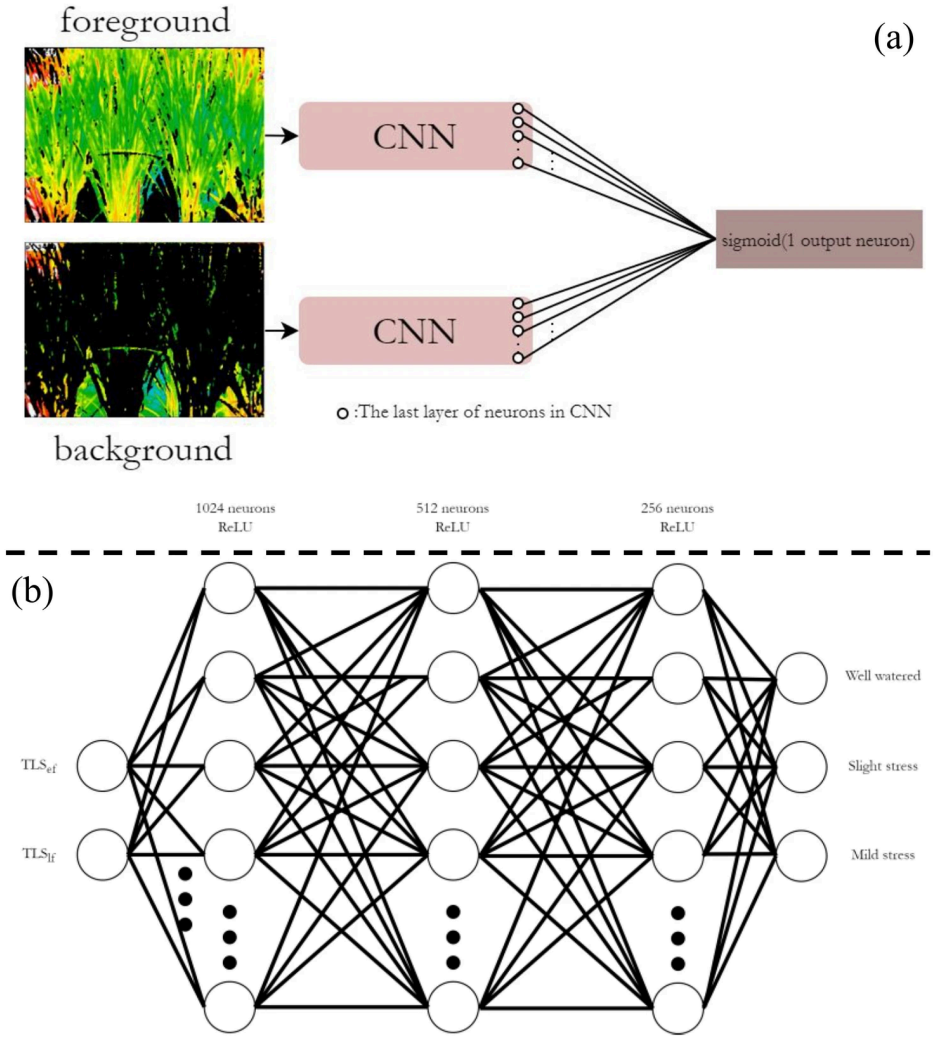



**Figure 5.** CNN late fusion and MLP classification network in water stress identification using thermal infrared imagery: (**a**) obtaining water stress discrimination features via CNN late fusion after separately extracting features from foreground and background thermal images; (**b**) network structure fusing two types of thermal map features and utilising a multilayer perceptron to classify full water supply, mild stress, and moderate stress [102].

Data-driven models may simultaneously absorb soil and crop background effects. Therefore, it is necessary to clearly define their prediction targets and uncertainties. On moderately and highly sodic soils, thermal indicators and classification and regression trees (CART) predicted the grain yield of 18 wheat genotypes. The resulting $R^2$ values were 0.78 and 0.69, respectively. Highly sodic soils exacerbated water stress, limiting yield by approximately 40%. This indicates that the model simultaneously captured both soil salinity-alkalinity and water supply effects [105]. Supervised learning using cherry canopy thermal imagery predicted stomatal conductance and stem water potential. The correlation coefficients were 0.83 and 0.81, respectively. This demonstrates that machine learning can handle complex fruit tree canopies. However, it cannot eliminate the interactive effects

of meteorology, soil moisture, and canopy structure [106]. Future research should report independent validations and confidence intervals. Furthermore, it should trigger ground verification when uncertainty is high.

## 5. From Thermal Diagnosis to Precision Irrigation Decisions

Translating thermal maps into irrigation actions involves at least three judgements [107]. First, continuous thermal signals must be converted into trigger thresholds. Second, plant status must be combined with root-zone water storage and weather conditions to determine the required irrigation volume. Third, spatial field heterogeneity must be translated into management zones or variable-rate prescriptions that equipment can execute. If any of these elements is missing, thermal imaging may remain merely at the stage of identifying differences. Consequently, it would be difficult to achieve stable water-saving effects. This chapter discusses the dynamism of thresholds and the fusion of multi-source information. It also examines the feedback processes among sensing, decision-making, execution, and evaluation.

### *5.1. Irrigation Trigger Thresholds*

Irrigation trigger thresholds should correspond to acceptable physiological risks, rather than merely representing statistically detectable temperature differences. Exceedingly low thresholds can transform short-term, reversible temperature increases into frequent irrigation events. Conversely, overly high thresholds may cause the crop to miss sensitive periods of yield formation [108,109]. Rational thresholds require the clear specification of index algorithms, crop species and cultivars, growth stages, and soil water storage capacity. Target yield or quality, alongside the permissible degree of regulated deficit, must also be defined. When weather changes rapidly, it is additionally necessary to distinguish between single-time-point exceedances and continuously accumulated stress [110,111]. Therefore, thresholds are better suited to be formulated as decision rules that adjust with phenology, VPD, and recent irrigation history. They should not be treated as single, unvarying values throughout the year [112,113].

Field trials can provide a starting point for threshold setting. However, the numerical values themselves cannot be utilised independently of crop types, cultivars, and specific stress strategies. For Indian mustard, an optimal yield and the highest water use efficiency were achieved when approximately 30% of the total available water in the root zone was consumed. This corresponded to an average CWSI of 0.4 [114]. In continuous regulated deficit treatments across three almond cultivars, significant water savings were realised with minimal yield impacts when the CWSI, derived from cultivar-specific baselines, was between 0.12 and 0.15. This range corresponded to a canopy temperature increase of approximately 1 °C [115]. The differing threshold ranges between these two studies demonstrate that thresholds must be jointly calibrated with specific crops and management objectives.

Threshold rules should also consider spatial coverage and climatic adaptability. This prevents a disconnect between regional-scale observations and field-level decision-making. A novel satellite CWSI derived from eight Landsat 8 images yielded $R^2$ values of 0.49 to 0.85 and RMSE values of 0.12 to 0.29 against ground-based CWSI measurements. Regional scheduling can be implemented with minimal ground assistance; nevertheless, the model alters with canopy development and plant age [116]. In deficit-irrigated cotton, the stress-time method triggered irrigation earlier in the season when the CWSI was still low. In contrast, the stress-degree-hour method only initiated irrigation at higher stress stages [117]. In humid environments, an empirical rule was applied, triggering irrigation after canopy temperatures exceeded the predicted fully watered baseline for more than 3 h per day over two consecutive days. This allowed maize to achieve 85% of its maximum yield using

less than 50% of the standard irrigation volume. However, different crops still require temperature threshold adjustments of 0.5 to 1 °C [118]. Cumulative rules alter the timing of intervention. Thus, they must be selected in accordance with local climate conditions and production goals.

Dynamic thresholds can update in response to inter-daily weather patterns and plant status. Consequently, they are more suitable for automatic irrigation control. An automatic irrigation algorithm for apples was designed based on theoretical CWSI trends. It successfully maintained soil deficits within the fully watered range and reduced over-irrigation during cool, wet weather. The $R^2$ between midday CWSI and stem water potential reached 0.91 [119]. Figure 6a–c illustrate the operational process of this dynamic algorithm across three apple experimental plots. The blue dotted lines represent the midday CWSI. The red curves denote the dynamic irrigation threshold, which varies with time and environmental conditions. The columnar sections indicate the actual irrigation volumes applied. The periods circled by dashed lines correspond to key nodes identified by the algorithm for initiating or ceasing irrigation. This demonstrates that dynamic thresholds can adjust irrigation trigger timing based on continuous thermal signals, rather than relying on fixed temperature limits. An open-source thermal imaging software utilised CWSI thresholds of 0.4 and 0.7 to trigger potato irrigation. Instead of claiming exact agronomic equivalence due to a lack of statistical significance, actual field observations indicated that the 0.4 threshold treatment resulted in a marginal fresh tuber yield reduction of 4.4 to 5.2 t/ha compared to full irrigation. Relative to the full irrigation control (the denominator), the thermal trials saved 341.6 and 515.7 $m^3$/ha of water in the respective seasons [120]. Figure 6d–e compare the CWSI variations and irrigation volumes among three treatments—full irrigation, CWSI < 0.4, and CWSI < 0.7—across the two potato trials. The results indicate that a higher threshold permits the crop to endure greater thermal stress. Conversely, a lower threshold enables earlier irrigation triggers. Therefore, threshold selection requires a careful trade-off between yield risks and water-saving margins. The former approach exemplifies updating thresholds based on physiological trends, whereas the latter evaluates threshold efficacy via yield outcomes and water usage. Ultimately, thresholds only acquire genuine management significance when incorporated into actual control systems and validated by field results.

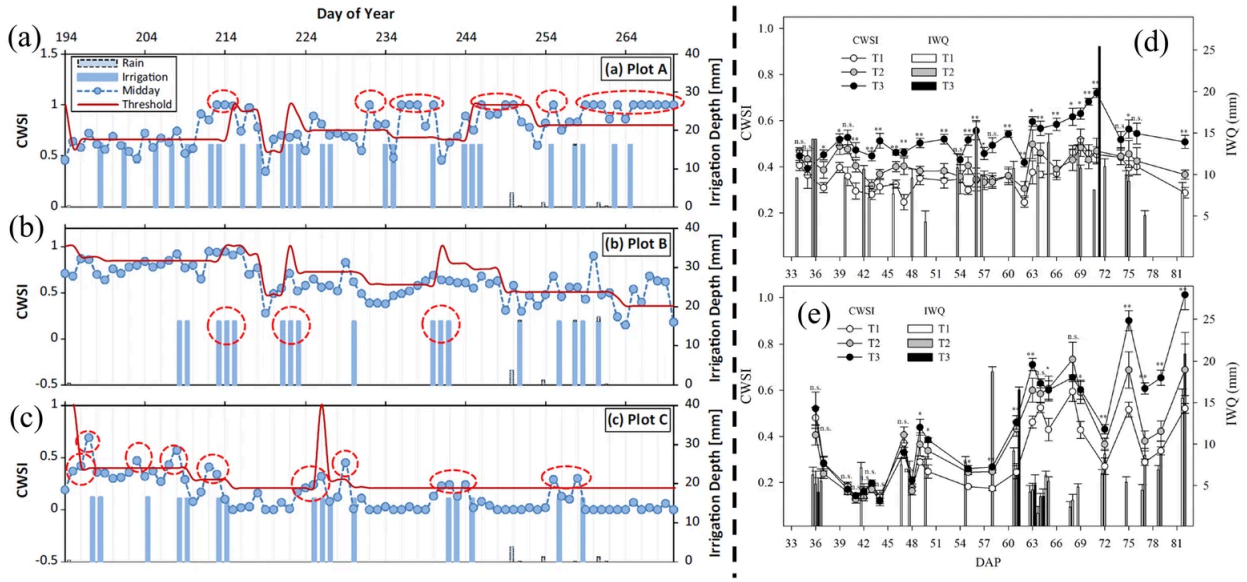



**Figure 6.** CWSI-based irrigation trigger thresholds and their dynamic control responses: (**a**–**c**) changes in irrigation triggering, cessation, and irrigation depth based on the dynamic CWSI threshold algorithm across three apple experimental plots [119]; (**d**,**e**) temporal variations of CWSI and irrigation

volume for potato under full irrigation, CWSI < 0.4, and CWSI < 0.7 treatments [120]. In panels (**d**,**e**), the symbols **, * and ns (n.s.) indicate $p < 0.01$, $p < 0.05$ and $p > 0.05$ (not significant), respectively, according to analysis of variance (ANOVA). DAP, days after planting; CWSI, crop water stress index; IWQ, irrigated water quantity.

### *5.2. Integration with Soil Moisture, Weather and Crop Models*

Thermal indicators reflect the comprehensive response of crops at the time of observation. Soil moisture describes root-zone storage. Meteorological data determine future evaporative demand. Meanwhile, crop or evapotranspiration models can extend this information to predict irrigation volumes and yield outcomes [121–124]. Relying on a single information source easily leads to ambiguity. For instance, when soil still retains water, plants may heat up due to root system or salinity constraints. Short-term canopy temperature increases might also stem from high VPD or cloud shadow variations [125–127]. The objective of information fusion is not simply to increase the number of variables. Rather, it utilises complementary information to distinguish among water source deficits, water transport limitations, and atmospheric demands. Ultimately, this transforms status diagnosis into a predictable water balance [127–129].

Plant responses and soil moisture do not always correspond linearly. Data assimilation can incorporate both types of information into continuous process estimations [130,131]. In a sugar beet field with significant spatial soil heterogeneity, UAV thermal imagery did not show a direct relationship with soil water content. However, higher plant stress identified via thermal imaging correlated with declines in fresh root weight and sugar content. The $R^2$ for the relationship with sugar content was 0.94 [132]. Microwave-thermal infrared coupled soil moisture profiles were assimilated into a regional DSSAT model using an ensemble Kalman filter. Consequently, the absolute error of yield estimation in rainfed areas decreased from approximately 36% to 29%. Irrigated counties still achieved an error of approximately 23%, even in the absence of irrigation management information [133]. Figure 7a,b display the time series of soil moisture differences for the rainfed and irrigated areas in this study. They simultaneously mark precipitation changes, the growing season range, and the corresponding yields. Soil moisture differences in rainfed areas primarily fluctuated in the short term alongside precipitation events. In contrast, irrigated areas exhibited more pronounced water replenishment and consumption processes during the growing season. This demonstrates that assimilating thermal infrared or microwave soil moisture information into crop models can convert instantaneous remote sensing observations into temporally continuous root-zone water and yield estimates. Remote sensing observations can thus continuously constrain crop processes, providing a basis for seasonal-scale predictions.

The effectiveness of multi-source fusion depends on whether the spatial scales represented by each variable align with the management unit. Observations of two pear cultivars showed that the correlation coefficient between raw canopy temperature and air temperature was as high as 0.99. Using raw canopy temperature alone is not robust. When stem water potential fell below −1.2 MPa, the CWSI and canopy-air temperature difference became more stable. The strength of their relationships with stem water potential ranked as follows: CWSI, canopy-air temperature difference, soil water content, and raw canopy temperature [134]. An Internet of Things (IoT) system in a vineyard integrated canopy temperature, weather, soil moisture, and irrigation volume into an edge-computing neural network. Over four consecutive years, CWSI remained significantly correlated with leaf water potential and available soil moisture [13]. Four years of grapevine data were analysed after adding meteorological variables. The $R^2$ of the single-plant model increased from 0.36 to 0.51. Meanwhile, the whole-vineyard model improved from 0.57 to 0.85 [135].

Fusion can reduce meteorological confounding. However, it must be validated at the scale of actual management units.

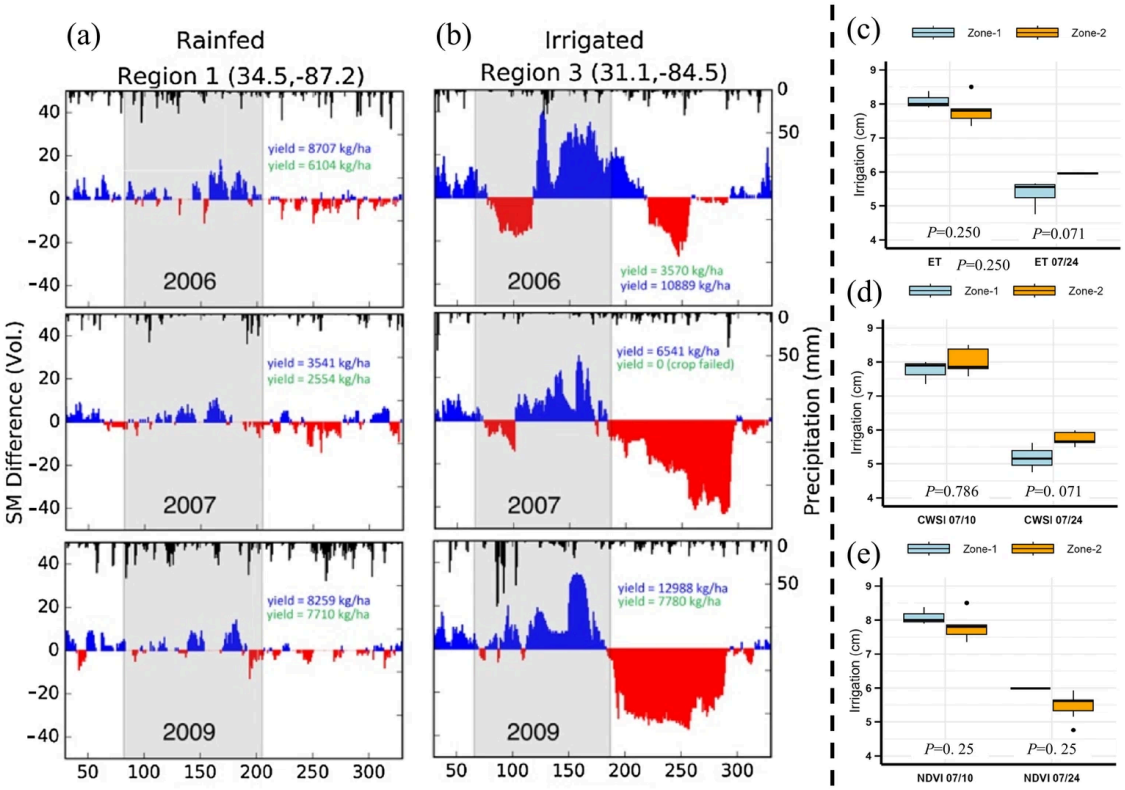



**Figure 7.** Soil-moisture differences, precipitation background, remote-sensing-based management zoning, and zonal irrigation-volume differences: (**a**,**b**) Soil-moisture differences, precipitation sequences, and yield responses in rainfed and irrigated regions, respectively. In these panels, blue and red areas indicate positive and negative soil-moisture differences, respectively, whereas the colored text denotes yield annotations [133]; (**c**) irrigation volumes in management zones delineated based on evapotranspiration; (**d**) irrigation volumes in management zones delineated based on CWSI; (**e**) irrigation volumes and their date differences in management zones delineated based on NDVI [14].

Multi-modal UAV data can further link evapotranspiration, plant water content, and water productivity. Nevertheless, each type of variable should bear a clear process-explanatory role. Multispectral data, thermal infrared imagery, point-cloud plant height, and leaf area index were inputted into a modified evapotranspiration model. Subsequently, a multi-modal random forest model for winter wheat predicted plant water content during the grain-filling stage with an $R^2$ of 0.900 and an nRMSE of 2.688%. Optimal water use efficiencies at different growth stages corresponded to varying water content thresholds [136]. Multi-sensor features, above-ground biomass, and SEBAL daily evapotranspiration jointly estimated maize biomass, evapotranspiration, and water use efficiency. The resulting $R^2$ values were 0.71, 0.93, and 0.79, respectively [137]. A relatively rational fusion framework would be as follows: thermal information constrains plant status and energy fluxes; soil sensors update available water storage; weather forecasts drive short-term demand; and crop models evaluate growth stages and yield risks.

### *5.3. Variable-Rate Irrigation, Feedback and Evaluation*

Variable-rate irrigation requires converting water status maps into prescription maps that match equipment control units. It also relies on sensor feedback for re-evaluation after execution [138–140]. Management zones are influenced by relatively stable factors

such as soil and topography. They also undergo intra-seasonal changes driven by root activity, canopy growth, and recent irrigation [141–143]. Evaluation should not merely stop at classification accuracy or the visual appearance of prescription maps. Instead, it should compare at least irrigation volumes, yield or quality, water productivity, spatial uniformity, response latency, and operational costs. Furthermore, model stability must be tested across wet years, dry years, and different crop types [144–146]. Systems should also record inputs, thresholds, and execution volumes for every decision to trace the sources of deviations.

Spatial thermal maps can be used to delineate variable-rate irrigation management zones. However, zoning results must undergo validation via irrigation and yield responses. Ground and aerial thermal scanning, combined with artificial wet references and the coldest 33% of pixels, constructed stress maps for cotton, processing tomatoes, and peanuts. For cotton, the $R^2$ between CWSI and leaf water potential reached 0.816. The spatial patterns aligned with farmer observations and irrigation history [147,148]. In an almond orchard, 11 flights capturing aerial multispectral and thermal imagery derived evapotranspiration, CWSI, and NDVI. K-means clustering identified two optimal zones for all indices. Evapotranspiration and CWSI explained the highest spatial variation at 73.6%. Their zoning consistency ranged from 0.84 to 1.00, outperforming approaches that rely solely on vegetative growth [14]. Figure 7c–e further compare the actual irrigation volumes in two regions after dividing management zones based on ET, CWSI, and NDVI. All three indicators could identify spatial irrigation differences on different dates. However, the magnitude and stability of the inter-zone differences were not entirely consistent. Among them, ET and CWSI demonstrated more direct connections with crop water consumption and stress status. In contrast, NDVI zoning was more susceptible to canopy growth and phenological changes. Thermal stress and evapotranspiration have a more direct relationship with the water supply process. Nonetheless, they cannot substitute for the validation of management outcomes.

The update frequency of dynamic zones should match crop change rates and equipment sampling capabilities [149]. A cotton variable-rate centre-pivot system utilised UAV-based NDVI weekly to describe early growth. It then used thermal imaging CWSI as a proxy for reproductive-stage leaf water potential. Compared to commercial uniform irrigation, static zoning and intra-seasonal dynamic zoning improved water productivity by 12% and 19%, respectively [150]. The sampling interval of a moving sprinkler was extended from 0.5 to 26 min. Intervals not exceeding 5 min had minor impacts on canopy temperature errors. The resulting management zones showed over 79% overlap with the most densely sampled results. However, the maximum overlap across different dates was only 67% [151]. In a 16-hectare commercial vineyard, remote sensing-based leaf water potential zones directed regulated deficit irrigation. It was recommended to acquire approximately 5 to 6 water potential maps within a season. After accounting for rainfall and low VPD, this strategy caused no negative effects on yield or wine composition [152].

Sensor feedback systems can now convert management zones into actual irrigation executions. Yet, their ultimate value must be evaluated under multi-year, field-scale, and equipment-constrained conditions [153–155]. Integrated CWSI feedback, a hybrid soil deficit-CWSI control, and manual neutron probe scheduling were evaluated against full irrigation (100% replenishment). Under a 75% replenishment level, the thermal plant-feedback system produced an observed seed cotton yield difference of +274 kg/ha relative to the manual full control, albeit with high variance (SE: 345 to 729). The minimum water savings in 2021 and 2022 were 20% and 16%, respectively (using the full irrigation treatment as the denominator) [156]. In a 58-hectare maize-soybean field, ISSCADA, SETMI, and conventional management were compared. Both decision systems involved infrared thermometers, soil sensors, weather stations, and satellites. They both successfully reduced

irrigation, with observed maize yield deviations of −0.6 t/ha under 50% deficit scheduling compared to full replenishment. To systematically evaluate the actual agronomic viability and yield risks of these thermal-based decisions, Table 1 details the comparator, water applied, absolute yield differences, and specific definitions of water productivity for key field trials. A 50% deficit level achieved the highest irrigation water productivity [157–159]. Variable-rate irrigation should align prescription update frequencies with equipment response scales. It should establish its acceptance criteria based on water savings without yield reduction, controllable risks, and acceptable maintenance costs [160–162].

**Table 1.** Agronomic outcomes and observed yield deviations of thermal-based irrigation management trials.

| Crop (Ref) | Year/ Experiment | Sample Size (*n*) | Comparator (Control) Irrigation & Yield | Thermal Treatment Irrigation & Yield | Water Applied & Savings (Denominator) | Yield Difference & Uncertainty | Water Productivity (WP) Definition (Strictly Matched to Original Studies) |
|---|---|---|---|---|---|---|---|
| Potato [120] | 2017–2018 seasons | $n = 4$ replications | Control: 1732 mm irrigation; Yield: 48.6 t/ha | Treatment: 1216.3 to 1390.4 mm; Yield: 43.4 to 44.2 t/ha | Saved 341.6 to 515.7 $m^3$/ha (10.5% to 29.7% of Control = 1732 $m^3$/ha) | −4.4 to −5.2 t/ha (± 0.38 SE) | Fresh tuber yield/ Total irrigation water applied [120] |
| Cotton [150] | 2022–2023 seasons | $n = 3$ blocks | Control (COM): 605 mm irrigation; Yield: 1380 kg/ha | Treatment: 517.8 mm; Yield: 1180 kg/ha | Saved 87.2 mm (14.4% of Control = 605 mm) | ~−200 ± 130 (SE) kg/ha | Cotton harvester yield/Total irrigation water applied [150] |
| Cotton [156] | 2021–2022 seasons | $n = 4$ field plots | Control (100% $ET_c$): 356 mm irrigation; Yield: 1820 kg/ha | Treatment (75% $ET_c$): 218 mm; Yield: 2094 kg/ha | Saved 138 mm (38.7% of Control = 356 mm) | +274 kg/ha (±65.4 SE) | (Seed yield—Rainfed yield)/Seasonal crop evapotranspiration ($ET_c$) [156] |
| Maize [157] | 2020–2021 seasons | $n = 3$ center pivots | Control (100% level): 236 mm irrigation; Yield: 12.4 t/ha | Treatment (50% deficit): 118 mm; Yield: 11.8 t/ha | Saved 118 mm (50.0% of Control = 236 mm) | −0.6 t/ha (±0.12 SE) | (Grain yield—Rainfed yield)/Total irrigation water depth [157] |

(Note: The absence of a statistically significant difference does not imply absolute agronomic equivalence; observed differences are reported alongside standard errors (SE) of the treatment means or differences to illustrate true agronomic yield risks. To prevent confounding internal treatment variability (standard deviations) with comparative uncertainty, all uncertainty measures explicitly represent the standard error of the mean differences or specific confidence intervals rather than pooled intra-treatment dispersion).

## 6. Conclusions and Research Priorities

Crop canopy temperature is jointly determined by root-zone water supply, plant hydraulic regulation, and atmospheric evaporative demand. Thermal infrared monitoring non-destructively translates stomatal closure and transpiration decline into continuous, mappable field signals. Its limitations also stem from this mechanism. Radiation, VPD, wind speed, canopy structure, and growth stage can all alter temperatures. Furthermore, salinity, nutrition, and diseases can induce temperature changes. Based on robust evidence across the synthesized studies, properly normalised temperature differences or CWSI consistently demonstrate reliable correlations with leaf water potential, stomatal conductance, soil moisture, evapotranspiration, and yield. These indices can subsequently be used for irrigation triggering, management zoning, and automatic feedback. However, the direct translation of these relationships into actionable irrigation thresholds is highly context-dependent. It relies heavily on the specific crop, cultivar, location, and season. Consequently, a single flight or a single static threshold is insufficient to support stable decision-making.

Reliable application depends on four categories of conditions. First, observation schemes should be determined by the decision scale. Fixed sensors are suitable for continuous early warning. UAVs are used for field zoning. Satellites are appropriate for regional screening. Meanwhile, handheld measurements can be used for calibration and anomaly verification. Second, radiometric calibration, drift correction, and thermal-visible image coregistration should be regarded as integral parts of the measurement model. Canopy segmentation and temperature statistics must also be included. It is particularly necessary

to control for mixed pixels containing soil and shadows. Third, the wet end, dry end, and non-stressed baselines of the CWSI must be validated according to crop, phenology, and meteorological conditions. Different algorithms require separately established thresholds. Fourth, model performance should be tested across independent years, locations, and management-unit scales. Errors and uncertainties must be reported simultaneously. This avoids mistaking high within-field data fitting for universal laws.

To address the limitation of poor cross-study comparability resulting from inconsistent methodologies, future research should prioritise the establishment of reproducible data specifications. These specifications should include camera parameters, emissivity, flight height, and time of day. Ground references, segmentation rules, meteorological synchronisation, and ground physiological measurements must also be detailed. Public datasets should not solely provide stitched and cropped temperature maps. They should also retain raw radiometric data, synchronised RGB or multispectral imagery, and calibration targets. Irrigation records and sample point coordinates should be included to allow new segmentation and calibration methods to be re-tested on the same baseline. Ground observations should cover a continuous gradient from full water supply to severe stress.

Furthermore, the specific temporal and spatial scales represented by leaf water potential, stem water potential, stomatal conductance, and soil water content must be explicitly defined. To overcome the limitation of static models failing under changing environments, proposals for future work must shift threshold setting from fixed constants to dynamic risk judgements. CWSI trends, stress duration, and growth stages should be jointly incorporated alongside available soil water and weather forecasts. Acceptable stress ranges should then be determined using yield, quality, and water productivity. Threshold outputs could adopt low, medium, and high-risk intervals. Concurrently, they should provide recommendations for continued observation, ground verification, or irrigation initiation. Multi-modal models should introduce energy balance and crop physiological constraints. They should conduct cross-regional external validation, domain shift detection, and confidence expression. When confidence is insufficient, manual or ground sensor verification should be requested. Cross-regional trials require pre-agreed independent test plots to avoid spatial leakage caused by random pixel splitting. They must separately report performance across different cultivars, phenological stages, weather conditions, and stress levels.

Research priorities should also expand from diagnostic accuracy to management efficacy. Long-term comparisons of uniform irrigation, static zoning, and dynamic variable-rate irrigation should be conducted in commercial fields. These comparisons should evaluate water use, revenue, energy consumption, maintenance burdens, and performance under extreme weather. Thermal infrared technology is better viewed as a decision-making system. This system should be centred on plant responses and constrained by soil moisture and meteorological information. Finally, it must interface seamlessly with irrigation equipment. Canopy temperature can only become a reliable basis for field-scale precision water management if it simultaneously satisfies the requirements of measurability, interpretability, transferability, and executability.

Finally, several limitations of this review itself must be acknowledged. First, the literature retrieval was primarily restricted to the Web of Science Core Collection, which limits the overall database coverage and may exclude relevant studies published in other indexing databases. Second, the selection process and the vast diversity of metrics used across different studies—ranging from single-leaf correlations to field-scale water productivity—complicated direct quantitative comparisons. Third, the absence of a standardized quality assessment protocol for the included studies means that varying levels of methodological rigor are presented. Furthermore, there is a potential publication bias toward favorable

results, as studies demonstrating successful thermal diagnostics or significant water savings are inherently more likely to be published than those reporting null or negative outcomes.

**Author Contributions:** Conceptualization, H.Z. and Z.T.; methodology, H.Z.; software, H.Z.; validation, H.Z. and Z.T.; formal analysis, H.Z.; investigation, H.Z.; resources, Z.T.; data curation, H.Z.; writing—original draft preparation, H.Z.; writing—review and editing, Z.T.; visualization, H.Z.; supervision, Z.T.; project administration, Z.T.; funding acquisition, Z.T. All authors have read and agreed to the published version of the manuscript.

**Funding:** This research was funded by the Postgraduate Research & Practice Innovation Program of Jiangsu Province, grant number KYCX25_4246; and the Ministry of Education, grant number MAET202326.

**Data Availability Statement:** No new data were created or analyzed in this study. Data sharing is not applicable to this article.

**Conflicts of Interest:** The authors declare no conflicts of interest.

## References

1. Berry, A.; Vivier, M.A.; Poblete-Echeverria, C. Evaluation of canopy fraction-based vegetation indices, derived from multispectral UAV imagery, to map water status variability in a commercial vineyard. *Irrig. Sci.* **2025**, *43*, 135–153. [CrossRef]
2. Noilhan, J.; Lacarrere, P. GCM Grid-Scale Evaporation from Mesoscale Modeling. *J. Clim.* **1995**, *8*, 206–223. [CrossRef]
3. Anderson, M.C.; Hain, C.R.; Jurecka, F.; Trnka, M.; Hlavinka, P.; Dulaney, W.; Otkin, J.A.; Johnson, D.; Gao, F. Relationships between the evaporative stress index and winter wheat and spring barley yield anomalies in the Czech Republic. *Clim. Res.* **2016**, *70*, 215–230. [CrossRef]
4. Costa, J.M.; Grant, O.M.; Chaves, M.M. Thermography to explore plant-environment interactions. *J. Exp. Bot.* **2013**, *64*, 3937–3949. [CrossRef] [PubMed]
5. Jones, H.G.; Hutchinson, P.A.; May, T.; Jamali, H.; Deery, D.M. A practical method using a network of fixed infrared sensors for estimating crop canopy conductance and evaporation rate. *Biosyst. Eng.* **2018**, *165*, 59–69. [CrossRef]
6. Song, L.S.; Liu, S.M.; Kustas, W.P.; Zhou, J.; Ma, Y.F. Using the Surface Temperature-Albedo Space to Separate Regional Soil and Vegetation Temperatures from ASTER Data. *Remote Sens.* **2015**, *7*, 5828–5848. [CrossRef]
7. Xiao, C.A.; Cai, J.B.; Zhang, B.Z.; Chang, H.F.; Wei, Z. Evaluation and verification of two evapotranspiration models based on precision screening and partitioning of field temperature data. *Agric. Water Manag.* **2023**, *278*, 108166. [CrossRef]
8. Maes, W.H.; Steppe, K. Estimating evapotranspiration and drought stress with ground-based thermal remote sensing in agriculture: A review. *J. Exp. Bot.* **2012**, *63*, 4671–4712. [CrossRef] [PubMed]
9. Vadivambal, R.; Jayas, D.S. Applications of Thermal Imaging in Agriculture and Food Industry-A Review. *Food Bioprocess Technol.* **2011**, *4*, 186–199. [CrossRef]
10. Zhou, Z.; Majeed, Y.; Naranjo, G.D.; Gambacorta, E.M.T. Assessment for crop water stress with infrared thermal imagery in precision agriculture: A review and future prospects for deep learning applications. *Comput. Electron. Agric.* **2021**, *182*, 106019. [CrossRef]
11. Ezenne, G.I.; Jupp, L.; Mantel, S.K.; Tanner, J.L. Current and potential capabilities of UAS for crop water productivity in precision agriculture. *Agric. Water Manag.* **2019**, *218*, 158–164. [CrossRef]
12. Barguache, H.; Ezzahar, J.; Khabba, S.; Elfarkh, J.; Er-Raki, S.; Chakir, A.; Jarlan, L.; Rafi, Z.; Fanise, P.; Le Dantec, V. Development of a new water stress index combining PRI and soil moisture for assessing olive tree water status in Morocco. *Remote Sens. Environ.* **2026**, *347*, 115676. [CrossRef]
13. King, B.A.; Shellie, K.C. A crop water stress index based internet of things decision support system for precision irrigation of wine grape. *Smart Agric. Technol.* **2023**, *4*, 100202. [CrossRef]
14. Sapkota, A.; Roby, M.; Peddinti, S.R.; Fulton, A.; Kisekka, I. Comparative analysis of evapotranspiration (ET), crop water stress index (CWSI), and normalized difference vegetation index (NDVI) to delineate site-specific irrigation management zones in almond orchards. *Sci. Hortic.* **2025**, *339*, 113860. [CrossRef]
15. Kubota, S.; Nishida, K.; Yoshida, S. A soil–plant–atmosphere continuum model reflecting the responses of plant hydraulic resistance to waterlogging. *J. Hydrol.* **2026**, *672*, 135402. [CrossRef]
16. Vernier, J.; Edouard, S.; Amiot, B.; Ferrand, M.; Tuzet, A.; Dupont, E.; Caruyer, C.; Iseghem, M.V.; Becker, A.; Combes, D.; et al. A Soil–Plant–Atmosphere Continuum model coupled to CFD to simulate plant energy and water exchanges in heterogeneous microclimates. *Agric. For. Meteorol.* **2026**, *376*, 110906. [CrossRef]

17. Shen, T.; Yang, K.; Li, Y.; Wang, P.; van Noordwijk, M.; Iqbal, S.; Josselin, F.; Li, Y.; Xu, J. Climate-resilient mountain orchard systems: A cross-scale framework linking microclimate regulation, energy-water balance, and G × E × M–EVH climate-risk management. *Agric. Syst.* **2027**, *240*, 104931. [CrossRef]
18. Zhang, K.; Zhu, G.; Ma, N.; Chen, H.; Shang, S. Improvement of evapotranspiration simulation in a physically based ecohydrological model for the groundwater–soil–plant–atmosphere continuum. *J. Hydrol.* **2022**, *613*, 128440. [CrossRef]
19. Anderson, M.C.; Kustas, W.P.; Norman, J.M.; Diak, G.T.; Hain, C.R.; Gao, F.; Yang, Y.; Knipper, K.R.; Xue, J.; Yang, Y.; et al. A brief history of the thermal IR-based Two-Source Energy Balance (TSEB) model–diagnosing evapotranspiration from plant to global scales. *Agric. For. Meteorol.* **2024**, *350*, 109951. [CrossRef]
20. Liu, X.; Xu, J.; Liu, B.; Wang, W.; Li, Y. A novel model of water-heat coupling for water-saving irrigated rice fields based on water and energy balance: Model formulation and verification. *Agric. Water Manag.* **2019**, *223*, 105705. [CrossRef]
21. Tunca, E.; Köksal, E.S.; Torres-Rua, A.; Kustas, W.P.; Nieto, H. Estimation of bell pepper evapotranspiration using two-source energy balance model based on high-resolution thermal and visible imagery from unmanned aerial vehicles. *J. Appl. Remote Sens.* **2022**, *16*, 022204. [CrossRef]
22. Albasha, R.; Manceau, L.; Webber, H.; Chelle, M.; Kimball, B.; Martre, P. MONTPEL: A multi-component Penman-Monteith energy balance model. *Agric. For. Meteorol.* **2024**, *358*, 110221. [CrossRef]
23. Yan, J.; Feng, X.; Zhang, X.; Zhao, L.; Sun, X.; Zhong, X.; Wang, Y. An energy balance-based vegetation microclimate process model: Enhanced accuracy in canopy temperature simulation. *Urban For. Urban Green.* **2025**, *113*, 129108. [CrossRef]
24. Chandel, A.K.; Khot, L.R.; Stöckle, C.O.; Kalcsits, L.; Mantle, S.; Rathnayake, A.P.; Peters, T.R. Canopy Transpiration Mapping in an Apple Orchard Using High-Resolution Airborne Spectral and Thermal Imagery with Weather Data. *AgriEngineering* **2025**, *7*, 154. [CrossRef]
25. Zhao, W.Y.; Dong, X.H.; Wu, Z.P.; Wei, C.; Li, L.; Yu, D.; Fan, X.; Ma, Y.M. Using infrared thermal imaging technology to estimate the transpiration rate of citrus trees and evaluate plant water status. *J. Hydrol.* **2022**, *615*, 15. [CrossRef]
26. Hou, M.J.; Tian, F.; Ortega-Farias, S.; Riveros-Burgos, C.; Zhang, T.; Lin, A.W. Estimation of crop transpiration and its scale effect based on ground and UAV thermal infrared remote sensing images. *Eur. J. Agron.* **2021**, *131*, 15. [CrossRef]
27. Wang, L.; Lin, M.W.; Han, Z.X.; Han, L.J.; He, L.; Sun, W.H. Simulating the Effects of Drought Stress Timing and the Amount Irrigation on Cotton Yield Using the CSM-CROPGRO-Cotton Model. *Agronomy* **2024**, *14*, 14. [CrossRef]
28. Zhang, W.X.; Wu, Q.; Sun, C.L.; Zhang, W.Y.; Ge, D.K.; Cao, J.; Yin, Y.J.; Li, H.; Cao, H.X. Biomass-based root morphological parameter models of rice (*Oryza sativa* L.) under different drought intensities and drought durations in juvenile differentiation stage. *Agron. J.* **2025**, *117*, e70205. [CrossRef]
29. Akhlaq, M.; Miao, H.L.; Zhang, C.; Yan, H.F.; Run, X.; Chauhdary, J.N.; Rehman, M.M.U.; Li, J.; Ren, J.T. Resilience Assessment of Tomato Crop Chlorophyll Fluorescence Against Water Stress Under Elevated $CO_2$ and Protective Cultivation. *Irrig. Drain.* **2025**, *74*, 1234–1252. [CrossRef]
30. Akhlaq, M.; Miao, H.L.; Zhang, C.; Xue, R.; Yan, H.F.; Hameed, M.U.; Li, J.; Ren, J.T.; Chauhdary, J.N.; Rehman, M.M.U. Response of tomato growth and transpiration under adequate elevated $CO_2$ concentrations coupled with irrigation regimes. *Irrig. Sci.* **2025**, *43*, 1651–1667. [CrossRef]
31. Quispe-Puma, M.R.; Xing, D.K.; Wu, Y.Y.; Zhang, Q.; Wang, J. Dynamic characteristics of leaf intracellular water, nutrients, metabolic energy, and photosynthetic responses to drought stress in maize. *Chil. J. Agric. Res.* **2025**, *85*, 677–688. [CrossRef]
32. Wu, K.K.; Li, X.Y.; Gao, C.; Li, X.; Zhao, Y.H.; Li, X.Y.; Sun, W.H. Physiological and Transcriptomic Responses of Xinjiang Wheat 'Xindong 22' (*Triticum aestivum* L.) to Drought Stress During Early Development. *Agriculture* **2026**, *16*, 483. [CrossRef]
33. Shabbir, A.; Mao, H.P.; Ullah, I.; Buttar, N.A.; Ajmal, M.; Lakhiar, I.A. Effects of Drip Irrigation Emitter Density with Various Irrigation Levels on Physiological Parameters, Root, Yield, and Quality of Cherry Tomato. *Agronomy* **2020**, *10*, 1685. [CrossRef]
34. Xue, R.; Zhang, C.; Yan, H.F.; Li, J.; Ren, J.T.; Akhlaq, M.; Hameed, M.U.; Disasa, K.N. Physiological Response of Tomato and Cucumber Plants to Micro-Spray in High-Temperature Environment: A Scientific and Effective Means of Alleviating Crop Heat Stress. *Agronomy* **2023**, *13*, 2798. [CrossRef]
35. Pipatsitee, P.; Eiumnoh, A.; Praseartkul, P.; Taota, K.; Kongpugdee, S.; Sakulleerungroj, K.; Cha-um, S. Application of infrared thermography to assess cassava physiology under water deficit condition. *Plant Prod. Sci.* **2018**, *21*, 398–406. [CrossRef]
36. Watanabe, K.; Agarie, H.; Aparatana, K.; Mitsuoka, M.; Taira, E.; Ueno, M.; Kawamitsu, Y. Fundamental Study on Water Stress Detection in Sugarcane Using Thermal Image Combined with Photosynthesis Measurement Under a Greenhouse Condition. *Sugar Tech* **2022**, *24*, 1382–1390. [CrossRef]
37. Ramos-Fernández, L.; Gonzales-Quiquia, M.; Huanuqueño-Murillo, J.; Tito-Quispe, D.; Heros-Aguilar, E.; del Pino, L.F.; Torres-Rua, A. Water Stress Index and Stomatal Conductance under Different Irrigation Regimes with Thermal Sensors in Rice Fields on the Northern Coast of Peru. *Remote Sens.* **2024**, *16*, 796. [CrossRef]
38. Hou, M.J.; Tian, F.; Zhang, T.; Huang, M.S. Evaluation of canopy temperature depression, transpiration, and canopy greenness in relation to yield of soybean at reproductive stage based on remote sensing imagery. *Agric. Water Manag.* **2019**, *222*, 182–192. [CrossRef]

39. Bhatti, S.; Heeren, D.M.; Evett, S.R.; O'Shaughnessy, S.A.; Rudnick, D.R.; Franz, T.E.; Ge, Y.F.; Neale, C.M.U. Crop response to thermal stress without yield loss in irrigated maize and soybean in Nebraska. *Agric. Water Manag.* **2022**, *274*, 107946. [CrossRef]
40. Baker, J.T.; Gitz, D.C.; Payton, P.; Wanjura, D.F.; Upchurch, D.R. Using leaf gas exchange to quantify drought in cotton irrigated based on canopy temperature measurements. *Agron. J.* **2007**, *99*, 637–644. [CrossRef]
41. Chauhdary, J.N.; Li, H.; Pan, X.W.; Zaman, M.; Anjum, S.A.; Yang, F.; Akbar, N.; Azamat, U. Modeling effects of climate change on crop phenology and yield of wheat-maize cropping system and exploring sustainable solutions. *J. Sci. Food Agric.* **2025**, *105*, 3679–3700. [CrossRef] [PubMed]
42. Yu, Q.H.; Kang, S.Z.; Wu, H.; Song, J.; Wang, H.; Parsons, D. Optimizing regional irrigation management in arid saline areas using a process-based hydro-salt-crop model and fallow strategy. *Agric. Water Manag.* **2025**, *320*, 109832. [CrossRef]
43. Maguire, M.S.; Neale, C.M.U.; Woldt, W.E. Improving Accuracy of Unmanned Aerial System Thermal Infrared Remote Sensing for Use in Energy Balance Models in Agriculture Applications. *Remote Sens.* **2021**, *13*, 1635. [CrossRef]
44. Qin, W.L.; Wang, J.; Ma, L.F.; Wang, F.; Hu, N.Y.; Yang, X.Y.; Xiao, Y.Y.; Zhang, Y.H.; Sun, Z.C.; Wang, Z.M.; et al. UAV-Based Multi-Temporal Thermal Imaging to Evaluate Wheat Drought Resistance in Different Deficit Irrigation Regimes. *Remote Sens.* **2022**, *14*, 5608. [CrossRef]
45. Gu, S.J.; Liao, Q.; Gao, S.Y.; Kang, S.Z.; Du, T.S.; Ding, R.S. Crop Water Stress Index as a Proxy of Phenotyping Maize Performance under Combined Water and Salt Stress. *Remote Sens.* **2021**, *13*, 4710. [CrossRef]
46. Dhara, S.; Ranjan, R.; Sahoo, R.N.; Pramanik, M.; Mukherjee, J.; Kumar, M.; Upadhyay, P.K.; Kumar, S. Drone thermal imaging for assessing water status response of variable nitrogen and water application in wheat. *Plant Physiol. Rep.* **2025**, *30*, 224–235. [CrossRef]
47. Ashfaq, W.; Brodie, G.; Fuentes, S.; Gupta, D. Infrared Thermal Imaging and Morpho-Physiological Indices Used for Wheat Genotypes Screening under Drought and Heat Stress. *Plants* **2022**, *11*, 3269. [CrossRef] [PubMed]
48. Stoll, M.; Schultz, H.R.; Berkelmann-Loehnertz, B. Exploring the sensitivity of thermal imaging for Plasmopara viticola pathogen detection in grapevines under different water status. *Funct. Plant Biol.* **2008**, *35*, 281–288. [CrossRef] [PubMed]
49. Ramos-Fernández, L.; Peralta-Graciano, K.G.; Quispe-Tito, D.J.; Hurtado-Leo, L.; Veramendi-Hidalgo, T. Water stress and NPK levels in cotton (*Gossypium barbadense* L.) detection using thermal imaging. *Agron. Mesoam.* **2025**, *36*, jf693w79. [CrossRef]
50. Yang, N.; Yuan, M.F.; Wang, P.; Zhang, R.B.; Sun, J.; Mao, H.P. Tea diseases detection based on fast infrared thermal image processing technology. *J. Sci. Food Agric.* **2019**, *99*, 3459–3466. [CrossRef] [PubMed]
51. Wu, Y.L.; Yuan, S.Q.; Zhu, J.J.; Tang, Y.; Tang, L.D. Estimation of Wheat Leaf Water Content Based on UAV Hyper-Spectral Remote Sensing and Machine Learning. *Agriculture* **2025**, *15*, 1898. [CrossRef]
52. Noguera, M.; Millán, B.; Pérez-Paredes, J.J.; Ponce, J.M.; Aquino, A.; Andújar, J.M. A New Low-Cost Device Based on Thermal Infrared Sensors for Olive Tree Canopy Temperature Measurement and Water Status Monitoring. *Remote Sens.* **2020**, *12*, 723. [CrossRef]
53. Petrie, P.R.; Wang, Y.N.; Liu, S.; Lam, S.; Whitty, M.A.; Skewes, M.A. The accuracy and utility of a low cost thermal camera and smartphone-based system to assess grapevine water status. *Biosyst. Eng.* **2019**, *179*, 126–139. [CrossRef]
54. Gutiérrez, S.; Fernández-Novales, J.; Diago, M.P.; Iñiguez, R.; Tardaguila, J. Assessing and mapping vineyard water status using a ground mobile thermal imaging platform. *Irrig. Sci.* **2021**, *39*, 457–468. [CrossRef]
55. Nugroho, A.P.; Wiratmoko, A.; Nugraha, D.; Markumningsih, S.; Sutiarso, L.; Falah, M.A.F.; Okayasu, T. Development of a low-cost thermal imaging system for water stress monitoring in indoor farming. *Smart Agric. Technol.* **2025**, *11*, 101048. [CrossRef]
56. Mangus, D.L.; Sharda, A.; Zhang, N.Q. Development and evaluation of thermal infrared imaging system for high spatial and temporal resolution crop water stress monitoring of corn within a greenhouse. *Comput. Electron. Agric.* **2016**, *121*, 149–159. [CrossRef]
57. Gonzalez-Dugo, V.; Zarco-Tejada, P.; Nicolás, E.; Nortes, P.A.; Alarcón, J.J.; Intrigliolo, D.S.; Fereres, E. Using high resolution UAV thermal imagery to assess the variability in the water status of five fruit tree species within a commercial orchard. *Precis. Agric.* **2013**, *14*, 660–678. [CrossRef]
58. Foody, G.M.; Arora, M.K. Incorporating mixed pixels in the training, allocation and testing stages of supervised classifications. *Pattern Recognit. Lett.* **1996**, *17*, 1389–1398. [CrossRef]
59. Gui, Y.F.; Tao, J.F. The recognition and decomposition of mixed pixels in the remotely sensed images based on gray system theory. In Proceedings of the International Symposium on Distributed Computing and Applications to Business, Engineering and Sciences, Wuhan, China, 13–16 September 2004; pp. 934–936.
60. Raj, A.; Minz, S. Game Theory Based Pixel Approximation for Remote Sensing Imagery. *Appl. Soft. Comput.* **2020**, *93*, 15. [CrossRef]
61. Liu, L.F.; Wang, B.; Zhang, L.M.; Zhang, J.Q. Decomposition of mixed pixels using Bayesian Self-Organizing Map (BSOM) neural networks. In Proceedings of the IEEE International Geoscience and Remote Sensing Symposium (IGARSS), Barcelona, Spain, 23–27 July 2007; pp. 2014–2017.

62. Tao, X.T.; Wang, B.; Zhang, L.M.; Zhang, J.Q. A new scheme for decomposition of mixed pixels based on nonnegative matrix factorization. In Proceedings of the IEEE International Geoscience and Remote Sensing Symposium (IGARSS), Barcelona, Spain, 23–27 July 2007; pp. 1759–1762.
63. Yu, B.H.; Chi, K.H. Support Vector Machine Classification Using Training Sets of Small Mixed Pixels: An Appropriateness Assessment of IKONOS Imagery. *Korean J. Remote Sens.* **2008**, *24*, 507–515.
64. Ibrahim, M.A.; Arora, M.K.; Ghosh, S.K. Improving the quality of remotely sensed derived land cover maps by incorporating mixed pixels in various stages of a supervised classification process. In Proceedings of the 23rd International Geoscience and Remote Sensing Symposium (IGARSS 2003), Toulouse, France, 21–25 July 2003; pp. 3447–3449.
65. Jin, J.; Wang, B.; Zhang, L.M. A Novel Approach Based on Fisher Discriminant Null Space for Decomposition of Mixed Pixels in Hyperspectral Imagery. *IEEE Geosci. Remote Sens. Lett.* **2010**, *7*, 699–703. [CrossRef]
66. Wang, B.; Zhou, H.; Zhang, L.M. Blind decomposition of mixed pixels using constrained non-negative matrix factorization. In Proceedings of the 25th IEEE International Geoscience and Remote Sensing Symposium (IGARSS 2005), Seoul, Republic of Korea, 25–29 July 2005; pp. 3757–3760.
67. Gerchow, M.; Kühnhammer, K.; Iraheta, A.; Marshall, J.D.; Beyer, M. Enhanced flight planning and calibration for UAV based thermal imaging: Implications for canopy temperature and transpiration analysis. *Front. For. Glob. Change* **2025**, *8*, 1457762. [CrossRef]
68. Han, Y.; Tarakey, B.A.; Hong, S.J.; Kim, S.Y.; Kim, E.; Lee, C.H.; Kim, G. Calibration and Image Processing of Aerial Thermal Image for UAV Application in Crop Water Stress Estimation. *J. Sens.* **2021**, *2021*, 14. [CrossRef]
69. Katz, L.; Ben-Gal, A.; Litaor, M.I.; Naor, A.; Peeters, A.; Goldshtein, E.; Lidor, G.; Keisar, O.; Marzuk, S.; Alchanatis, V.; et al. How Sensitive Is Thermal Image-Based Orchard Water Status Estimation to Canopy Extraction Quality? *Remote Sens.* **2023**, *15*, 1448. [CrossRef]
70. Meron, M.; Sprintsin, M.; Tsipris, J.; Alchanatis, V.; Cohen, Y. Foliage temperature extraction from thermal imagery for crop water stress determination. *Precis. Agric.* **2013**, *14*, 467–477. [CrossRef]
71. Zhang, L.; Chen, P.; Ma, R.; He, M.; Zhu, H.; Lan, Y. A pixel-aligned co-registration and DSM-grid fusion framework for UAV multispectral and thermal imagery and point-cloud data: 3D Characterization of crop canopy water status. *Comput. Electron. Agric.* **2026**, *241*, 111290. [CrossRef]
72. Poblete, T.; Ortega-Farías, S.; Ryu, D. Automatic Coregistration Algorithm to Remove Canopy Shaded Pixels in UAV-Borne Thermal Images to Improve the Estimation of Crop Water Stress Index of a Drip-Irrigated Cabernet Sauvignon Vineyard. *Sensors* **2018**, *18*, 397. [CrossRef] [PubMed]
73. Zhang, L.Y.; Niu, Y.X.; Zhang, H.H.; Han, W.T.; Li, G.; Tang, J.D.; Peng, X.S. Maize Canopy Temperature Extracted From UAV Thermal and RGB Imagery and Its Application in Water Stress Monitoring. *Front. Plant Sci.* **2019**, *10*, 1270. [CrossRef] [PubMed]
74. Wang, X.X.; Wang, B.Y.; Yan, H.F.; Zhang, C.; Zheng, H.X.; Wang, G.Q.; Zhang, J.Y.; Bao, R.X.; Xue, R.; Zhou, Y.D.; et al. Comparison of four upscaling methods to drive instantaneous evapotranspiration to daily values for maize in two climatic regions in China. *J. Agric. Sci.* **2024**, *162*, 539–552. [CrossRef]
75. Zhang, C.; Li, L.L.; Yan, H.F.; Ou, M.X.; Akhlaq, M.; Zhang, W.C.; Huang, S. Calibration and validation of three evapotranspiration models in a tea field in the humid region of south-east China. *Irrig. Drain.* **2022**, *71*, 1254–1267. [CrossRef]
76. Bellvert, J.; Marsal, J.; Girona, J.; Gonzalez-Dugo, V.; Fereres, E.; Ustin, S.L.; Zarco-Tejada, P.J. Airborne Thermal Imagery to Detect the Seasonal Evolution of Crop Water Status in Peach, Nectarine and Saturn Peach Orchards. *Remote Sens.* **2016**, *8*, 39. [CrossRef]
77. Santesteban, L.G.; Di Gennaro, S.F.; Herrero-Langreo, A.; Miranda, C.; Royo, J.B.; Matese, A. High-resolution UAV-based thermal imaging to estimate the instantaneous and seasonal variability of plant water status within a vineyard. *Agric. Water Manag.* **2017**, *183*, 49–59. [CrossRef]
78. Hoffmann, H.; Jensen, R.; Thomsen, A.; Nieto, H.; Rasmussen, J.; Friborg, T. Crop water stress maps for an entire growing season from visible and thermal UAV imagery. *Biogeosciences* **2016**, *13*, 6545–6563. [CrossRef]
79. Ben-Gal, A.; Agam, N.; Alchanatis, V.; Cohen, Y.; Yermiyahu, U.; Zipori, I.; Presnov, E.; Sprintsin, M.; Dag, A. Evaluating water stress in irrigated olives: Correlation of soil water status, tree water status, and thermal imagery. *Irrig. Sci.* **2009**, *27*, 367–376. [CrossRef]
80. Cohen, Y.; Alchanatis, V.; Saranga, Y.; Rosenberg, O.; Sela, E.; Bosak, A. Mapping water status based on aerial thermal imagery: Comparison of methodologies for upscaling from a single leaf to commercial fields. *Precis. Agric.* **2017**, *18*, 801–822. [CrossRef]
81. Barai, K.; Wallhead, M.; Hall, B.; Rahimzadeh-Bajgiran, P.; Meireles, J.; Herrmann, I.; Zhang, Y.J. Detecting spatial variation in wild blueberry water stress using UAV-borne thermal imagery: Distinct temporal and reference temperature effects. *Precis. Agric.* **2025**, *26*, 25. [CrossRef]
82. Cohen, Y.; Alchanatis, V.; Meron, M.; Saranga, Y.; Tsipris, J. Estimation of leaf water potential by thermal imagery and spatial analysis. *J. Exp. Bot.* **2005**, *56*, 1843–1852. [CrossRef] [PubMed]
83. Wanjura, D.F.; Upchurch, D.R. Canopy temperature characterizations of corn and cotton water status. *Trans. ASAE* **2000**, *43*, 867–875. [CrossRef]

84. DeJonge, K.C.; Taghvaeian, S.; Trout, T.J.; Comas, L.H. Comparison of canopy temperature-based water stress indices for maize. *Agric. Water Manag.* **2015**, *156*, 51–62. [CrossRef]
85. Khorsandi, A.; Hemmat, A.; Mireei, S.A.; Amirfattahi, R.; Ehsanzadeh, P. Plant temperature-based indices using infrared thermography for detecting water status in sesame under greenhouse conditions. *Agric. Water Manag.* **2018**, *204*, 222–233. [CrossRef]
86. Han, M.; Zhang, H.H.; DeJonge, K.C.; Comas, L.H.; Trout, T.J. Estimating maize water stress by standard deviation of canopy temperature in thermal imagery. *Agric. Water Manag.* **2016**, *177*, 400–409. [CrossRef]
87. Luan, Y.J.; Xu, J.Z.; Lv, Y.P.; Liu, X.Y.; Wang, H.Y.; Liu, S.M. Improving the performance in crop water deficit diagnosis with canopy temperature spatial distribution information measured by thermal imaging. *Agric. Water Manag.* **2021**, *246*, 106699. [CrossRef]
88. Katimbo, A.; Rudnick, D.R.; DeJonge, K.C.; Lo, T.H.; Qiao, X.; Franz, T.E.; Nakabuye, H.N.; Duan, J. Crop water stress index computation approaches and their sensitivity to soil water dynamics. *Agric. Water Manag.* **2022**, *266*, 107575. [CrossRef]
89. Taghvaeian, S.; Comas, L.; DeJonge, K.C.; Trout, T.J. Conventional and simplified canopy temperature indices predict water stress in sunflower. *Agric. Water Manag.* **2014**, *144*, 69–80. [CrossRef]
90. Liu, Q.; Hu, X.L.; Zhang, Y.Q.; Shi, L.S.; Yang, W.; Yang, Y.X.; Zhang, R.X.; Zhang, D.L.; Miao, Z.; Wang, Y.F.; et al. Improving maize water stress diagnosis accuracy by integrating multimodal UAVs data and leaf area index inversion model. *Agric. Water Manag.* **2025**, *312*, 109407. [CrossRef]
91. Rossi, H.; Cherif, E.; Azzirgue, E.; El Azhari, H.; Boulaassal, H.; El Kharki, O. Remote Sensing for Irrigation Water Management Under Climate Change: Advances, Challenges, and Future Directions. *Climate* **2026**, *14*, 124. [CrossRef]
92. Mertens, S.; Verbraeken, L.; Sprenger, H.; De Meyer, S.; Demuynck, K.; Cannoot, B.; Merchie, J.; De Block, J.; Vogel, J.T.; Bruce, W.; et al. Monitoring of drought stress and transpiration rate using proximal thermal and hyperspectral imaging in an indoor automated plant phenotyping platform. *Plant Methods* **2023**, *19*, 25. [CrossRef] [PubMed]
93. Zhang, L.Y.; Zhang, H.H.; Zhu, Q.Z.; Niu, Y.X. Further investigating the performance of crop water stress index for maize from baseline fluctuation, effects of environmental factors, and variation of critical value. *Agric. Water Manag.* **2023**, *285*, 108349. [CrossRef]
94. Gonzalez-Dugo, V.; Zarco-Tejada, P.J.; Fereres, E. Applicability and limitations of using the crop water stress index as an indicator of water deficits in citrus orchards. *Agric. For. Meteorol.* **2014**, *198–199*, 94–104. [CrossRef]
95. Egea, G.; Padilla-Díaz, C.M.; Martinez-Guanter, J.; Fernández, J.E.; Pérez-Ruiz, M. Assessing a crop water stress index derived from aerial thermal imaging and infrared thermometry in super-high density olive orchards. *Agric. Water Manag.* **2017**, *187*, 210–221. [CrossRef]
96. Zoratipour, E.; Veysi, S.; Mohammadi, A.S.; Nasab, S.B.; Naseri, A. Deriving hourly and daily crop water stress index through the lens of proximal sensing in sugarcane fields. *Ain Shams Eng. J.* **2026**, *17*, 103903. [CrossRef]
97. Kumar, N.; Shankar, V.; Rustum, R.; Adeloye, A.J. Evaluating the Performance of Self-Organizing Maps to Estimate Well-Watered Canopy Temperature for Calculating Crop Water Stress Index in Indian Mustard (*Brassica juncea*). *J. Irrig. Drain. Eng.-ASCE* **2021**, *147*, 04020040. [CrossRef]
98. Apolo-Apolo, O.E.; Martínez-Guanter, J.; Pérez-Ruiz, M.; Egea, G. Design and assessment of new artificial reference surfaces for real time monitoring of crop water stress index in maize. *Agric. Water Manag.* **2020**, *240*, 106304. [CrossRef]
99. Poirier-Pocovi, M.; Volder, A.; Bailey, B.N. Modeling of reference temperatures for calculating crop water stress indices from infrared thermography. *Agric. Water Manag.* **2020**, *233*, 106070. [CrossRef]
100. Wang, J.J.; Lou, Y.; Wang, W.T.; Liu, S.Y.; Zhang, H.H.; Hui, X.; Wang, Y.L.; Yan, H.J.; Maes, W.H. A robust model for diagnosing water stress of winter wheat by combining UAV multispectral and thermal remote sensing. *Agric. Water Manag.* **2024**, *291*, 108616. [CrossRef]
101. Mali, S.S.; Scobie, M.; Baillie, J.; Plant, C.; Shammi, S.; Das, A. Integrating UAV-based multispectral and thermal infrared imageries with machine learning for predicting water stress in winter wheat. *Precis. Agric.* **2025**, *26*, 44. [CrossRef]
102. Li, M.-W.; Chan, Y.-K.; Yu, S.-S. Use of CNN for Water Stress Identification in Rice Fields Using Thermal Imagery. *Appl. Sci.* **2023**, *13*, 5423. [CrossRef]
103. Melo, L.L.d.; Melo, V.G.M.L.d.; Marques, P.A.A.; Frizzone, J.A.; Coelho, R.D.; Romero, R.A.F.; Barros, T.H.d.S. Deep learning for identification of water deficits in sugarcane based on thermal images. *Agric. Water Manag.* **2022**, *272*, 107820. [CrossRef]
104. Zhang, X.M.; Guan, H.W.; Zhao, J.L.; Suo, L.N.; Li, D.Y.; Ma, Z.Y.; Duan, J.Z.; He, L.; Liu, W.D.; Feng, W. Drought resistance classification of wheat varieties by multisource data fusion and machine learning via hyperspectral and thermal infrared imaging. *Chem. Biol. Technol. Agric.* **2025**, *12*, 165. [CrossRef]
105. Das, S.; Christopher, J.; Apan, A.; Choudhury, M.R.; Chapman, S.; Menzies, N.W.; Dang, Y.P. Evaluation of water status of wheat genotypes to aid prediction of yield on sodic soils using UAV-thermal imaging and machine learning. *Agric. For. Meteorol.* **2021**, *307*, 108477. [CrossRef]

106. Carrasco-Benavides, M.; Gonzalez Viejo, C.; Tongson, E.; Baffico-Hernández, A.; Ávila-Sánchez, C.; Mora, M.; Fuentes, S. Water status estimation of cherry trees using infrared thermal imagery coupled with supervised machine learning modeling. *Comput. Electron. Agric.* **2022**, *200*, 107256. [CrossRef]
107. Zhang, M.N.; Zhao, W.X.; Zhu, C.X.; Li, J.S. Influence of the sampling time interval of canopy temperature on the dynamic zoning of variable rate irrigation. *Agric. Water Manag.* **2024**, *295*, 108754. [CrossRef]
108. Lu, Y.Z.; Zheng, J.L.; Hu, H.J.; Pan, Q.M.; Cui, L.F.; Hu, Y.G. Determination of Critical Crop Water Stress Index of Tea under Drought Stress Based on the Intercellular $CO_2$ Concentration. *Agronomy* **2024**, *14*, 2154. [CrossRef]
109. Zou, Y.F.; Saddique, Q.; Ali, A.; Xu, J.T.; Khan, M.I.; Qing, M.; Azmat, M.; Cai, H.J.; Siddique, K.H.M. Deficit irrigation improves maize yield and water use efficiency in a semi-arid environment. *Agric. Water Manag.* **2021**, *243*, 106483. [CrossRef]
110. Ullah, I.; Mao, H.P.; Rasool, G.; Gao, H.Y.; Javed, Q.; Sarwar, A.; Khan, M.I. Effect of Deficit Irrigation and Reduced N Fertilization on Plant Growth, Root Morphology and Water Use Efficiency of Tomato Grown in Soilless Culture. *Agronomy* **2021**, *11*, 228. [CrossRef]
111. Chauhdary, J.N.; Li, H.; Ragab, R.; Hussain, Z.; Anjum, S.A.; Llxomovich, M.K. Modeling wheat growth to determine economic feasibility under deficit irrigation and nitrogen management strategies. *Agric. Water Manag.* **2025**, *319*, 109740. [CrossRef]
112. Gao, C.; Lin, M.W.; He, L.; Tang, M.R.; Ma, J.N.; Sun, W.H. The Impact of Water-Saving Irrigation on Rice Growth and Comprehensive Evaluation of Irrigation Strategies. *Agronomy* **2024**, *14*, 1363. [CrossRef]
113. Wang, X.W.; Cai, H.J.; Zheng, Z.; Yu, L.Y.; Wang, Z.S.; Li, L. Modelling root water uptake under deficit irrigation and rewetting in Northwest China. *Agron. J.* **2020**, *112*, 158–174. [CrossRef]
114. Kumar, N.; Poddar, A.; Shankar, V.; Ojha, C.S.P.; Adeloye, A.J. Crop water stress index for scheduling irrigation of Indian mustard (Brassica juncea) based on water use efficiency considerations. *J. Agron. Crop Sci.* **2020**, *206*, 148–159. [CrossRef]
115. Gutiérrez-Gordillo, S.; García-Tejero, I.F.; Durán Zuazo, V.H.; García Escalera, A.; Ferrera Gil, F.; Amores-Agüera, J.J.; Cárceles Rodríguez, B.; Hernández-Santana, V. Assessing the Water-Stress Baselines by Thermal Imaging for Irrigation Management in Almond Plantations under Water Scarcity Conditions. *Water* **2020**, *12*, 1298. [CrossRef]
116. Veysi, S.; Naseri, A.A.; Hamzeh, S.; Bartholomeus, H. A satellite based crop water stress index for irrigation scheduling in sugarcane fields. *Agric. Water Manag.* **2017**, *189*, 70–86. [CrossRef]
117. Baker, J.T.; Mahan, J.R.; Gitz, D.C.; Lascano, R.J.; Ephrath, J.E. Comparison of deficit irrigation scheduling methods that use canopy temperature measurements. *Plant Biosyst.* **2013**, *147*, 40–49. [CrossRef]
118. Bockhold, D.L.; Thompson, A.L.; Sudduth, K.A.; Henggeler, J.C. Irrigation Scheduling Based on Crop Canopy Temperature for Humid Environments. *Trans. Asabe* **2011**, *54*, 2021–2028. [CrossRef]
119. Osroosh, Y.; Troy Peters, R.; Campbell, C.S.; Zhang, Q. Automatic irrigation scheduling of apple trees using theoretical crop water stress index with an innovative dynamic threshold. *Comput. Electron. Agric.* **2015**, *118*, 193–203. [CrossRef]
120. Cucho-Padin, G.; Rinza, J.; Ninanya, J.; Loayza, H.; Quiroz, R.; Ramírez, D.A. Development of an Open-Source Thermal Image Processing Software for Improving Irrigation Management in Potato Crops (*Solanum tuberosum* L.). *Sensors* **2020**, *20*, 472. [CrossRef] [PubMed]
121. Yan, H.F.; Zhang, C.; Oue, H.; Peng, G.J.; Darko, R.O. Determination of crop and soil evaporation coefficients for estimating evapotranspiration in a paddy field. *Int. J. Agric. Biol. Eng.* **2017**, *10*, 130–139. [CrossRef]
122. Yan, H.F.; Acquah, S.J.; Zhang, J.Y.; Wang, G.Q.; Zhang, C.; Darko, R.O. Overview of modelling techniques for greenhouse microclimate environment and evapotranspiration. *Int. J. Agric. Biol. Eng.* **2021**, *14*, 1–8. [CrossRef]
123. Wang, B.Y.; Bao, R.X.; Yan, H.F.; Zheng, H.X.; Wu, J.B.; Zhang, C.; Wang, G.Q. Study of evapotranspiration and crop coefficients for eggplant in a Venlo-type greenhouse in South China. *Irrig. Drain.* **2025**, *74*, 556–568. [CrossRef]
124. Rasool, G.; Guo, X.P.; Wang, Z.C.; Ullah, I.; Chen, S. Effect of two types of irrigation on growth, yield and water productivity of maize under different irrigation treatments in an arid environment. *Irrig. Drain.* **2020**, *69*, 732–742. [CrossRef]
125. Yan, H.F.; Acquah, S.J.; Zhang, C.; Wang, G.Q.; Huang, S.; Zhang, H.N.; Zhao, B.S.; Wu, H.M. Energy partitioning of greenhouse cucumber based on the application of Penman-Monteith and Bulk Transfer models. *Agric. Water Manag.* **2019**, *217*, 201–211. [CrossRef]
126. Liu, Y.W.; Yan, H.F.; Zhang, C.; Zhang, J.Y.; Wang, G.Q.; Zhang, D.S.; Bao, R.X.; Wang, B.Y.; Zhou, Y.D.; Han, Y.J. Application of Evapotranspiration Models Coupled With Single and Dual-Source Hypotheses in Maize (*Zea mays* L.) Fields in Northwest and Northeast China. *J. Agron. Crop Sci.* **2026**, *212*, e70163. [CrossRef]
127. Zheng, H.X.; Wang, B.Y.; Wang, X.X.; Yan, H.F.; Wu, J.B.; Wang, G.Q.; Bao, R.X.; Hao, B.B.; Han, Y.J. Global sensitivity analysis of SIMDual-Kc for modeling evapotranspiration in maize field under film-mulched and drip irrigation. *Irrig. Sci.* **2025**, *43*, 1503–1519. [CrossRef]
128. Yan, H.F.; Yu, J.J.; Zhang, C.; Wang, G.Q.; Huang, S.; Ma, J.M. Comparison of two canopy resistance models to estimate evapotranspiration for tea and wheat in southeast China. *Agric. Water Manag.* **2021**, *245*, 106581. [CrossRef]

129. Yan, H.F.; Huang, S.; Zhang, J.Y.; Zhang, C.; Wang, G.Q.; Li, L.L.; Zhao, S.; Li, M.; Zhao, B.S. Comparison of Shuttleworth-Wallace and Dual Crop Coefficient Method for Estimating Evapotranspiration of a Tea Field in Southeast China. *Agriculture* **2022**, *12*, 1392. [CrossRef]
130. Jiang, J.H.; Wang, B.Y.; Yan, H.F.; Zhang, C.; Zhang, J.Y.; Wang, G.Q.; Liang, S.W.; Deng, S.S.; Zhou, Y.D. Improving Jarvis Canopy Resistance Model by Modifying the Effective Leaf Area Index in a Venlo-Type Greenhouse. *J. Agron. Crop Sci.* **2025**, *211*, 13. [CrossRef]
131. Abubaker, B.A.; Yan, H.F.; Hong, L.; You, W.Y.; Elshaikh, N.A.; Hussein, G.; Pandab, S.; Hassan, S. Enhancement of Depleted Loam Soil as Well as Cucumber Productivity Utilizing Biochar Under Water Stress. *Commun. Soil Sci. Plant Anal.* **2019**, *50*, 49–64. [CrossRef]
132. Quebrajo, L.; Perez-Ruiz, M.; Pérez-Urrestarazu, L.; Martínez, G.; Egea, G. Linking thermal imaging and soil remote sensing to enhance irrigation management of sugar beet. *Biosyst. Eng.* **2018**, *165*, 77–87. [CrossRef]
133. Mishra, V.; Cruise, J.F.; Mecikalski, J.R. Assimilation of coupled microwave/thermal infrared soil moisture profiles into a crop model for robust maize yield estimates over Southeast United States. *Eur. J. Agron.* **2021**, *123*, 126208. [CrossRef]
134. Blanco, V.; Willsea, N.; Campbell, T.; Howe, O.; Kalcsits, L. Combining thermal imaging and soil water content sensors to assess tree water status in pear trees. *Front. Plant Sci.* **2023**, *14*, 1197437. [CrossRef] [PubMed]
135. Bahat, I.; Netzer, Y.; Grünzweig, J.M.; Naor, A.; Alchanatis, V.; Ben-Gal, A.; Keisar, O.; Lidor, G.; Cohen, Y. How do spatial scale and seasonal factors affect thermal-based water status estimation and precision irrigation decisions in vineyards? *Precis. Agric.* **2024**, *25*, 1477–1501. [CrossRef]
136. Fu, W.; Hou, X.; Wang, D.; Chen, Z.; Cheng, Q.; Li, Y.; Duan, F. Monitoring plant moisture content and optimizing irrigation prescriptions based on UAV multimodal data. *Front. Plant Sci.* **2026**, *17*, 1827521. [CrossRef] [PubMed]
137. Chang, W.; Gu, S.; Wang, B.; Hu, S.; Li, R.; Guo, X. Estimating water use efficiency in maize: A UAV-based approach integrating multisensory data with SEBAL evapotranspiration modeling. *Comput. Electron. Agric.* **2025**, *237*, 110695. [CrossRef]
138. Liu, C.; Qi, Z.; Gu, Z.; Gui, D.; Zeng, F. Optimizing Irrigation Rates for Cotton Production in an Extremely Arid Area Using Rzwqm2-Simulated Water Stress. *Trans. Asabe* **2017**, *60*, 2041–2052. [CrossRef]
139. Li, L.; Liu, J.Z.; Peng, Q.; Wang, X.W.; Xu, J.T.; Cai, H.J. Propagation process-based agricultural drought typology and its copula-based risk. *Irrig. Drain.* **2024**, *73*, 1496–1519. [CrossRef]
140. Liu, Y.W.; Yan, H.F.; Zhang, C.; Zhang, J.Y.; Wang, G.Q.; Zhang, D.S.; Bao, R.X.; Han, Y.J. Application of Irrigation Decision-Making Methods for Smart Irrigation Systems: A Review. *Irrig. Drain.* **2026**, *75*, 1250–1264. [CrossRef]
141. Zhou, R.; Yan, H.F.; Zhang, C.; Zhu, X.Y.; Wang, G.Q.; He, B.; Disasa, K.N.; Lakhiar, I.A.; Xue, R.; Zhou, Y.D.; et al. Effects of alternating wet and dry irrigation regimes on rice growth and physiology characteristics in southeast China. *Paddy Water Environ.* **2025**, *23*, 301–321. [CrossRef]
142. Chen, Y.; Lin, M.W.; Yu, Z.; Sun, W.H.; Fu, W.G.; He, L. Enhancing cotton irrigation with distributional actor-critic reinforcement learning. *Agric. Water Manag.* **2025**, *307*, 14. [CrossRef]
143. Tunio, M.H.; Gao, J.M.; Talpur, M.A.; Lakhiar, I.A.; Chandio, F.A.; Shaikh, S.A.; Solangi, K.A. Effects of different irrigation frequencies and incorporation of rice straw on yield and water productivity of wheat crop. *Int. J. Agric. Biol. Eng.* **2020**, *13*, 138–145. [CrossRef]
144. Shi, R.C.; Han, X.B.; Guo, W.Z. Uncertain multi-objective programming approach for planning supplementary irrigation areas in rainfed agricultural regions. *Irrig. Drain.* **2025**, *74*, 1193–1214. [CrossRef]
145. Wang, L.; He, L.; Sun, W.H.; Gao, C.; Han, Z.X.; Lin, M.W. Precise irrigation of dryland cotton under canal irrigation system constraints based on the CERES-CROPGRO-Cotton model. *Agric. Water Manag.* **2025**, *317*, 14. [CrossRef]
146. Zhou, Y.D.; Bao, R.X.; Yan, H.F.; Zhang, C.; Zheng, H.X.; Wu, J.B.; Zhang, J.Y.; Wang, G.Q.; Tian, D.L.; Xue, R.; et al. Optimization of shallow buried drip irrigation and nitrogen management for spring maize in the sandy land of Northwest China. *Field Crops Res.* **2025**, *333*, 110056. [CrossRef]
147. Meron, M.; Tsipris, J.; Orlov, V.; Alchanatis, V.; Cohen, Y. Crop water stress mapping for site-specific irrigation by thermal imagery and artificial reference surfaces. *Precis. Agric.* **2010**, *11*, 148–162. [CrossRef]
148. Jiang, Y.; Li, B.Y.; Wang, X.Y.; Shi, B. Determination of optimal biochar application and irrigation rate for tomatoes based on the EWM-TOPSIS evaluation method. *Irrig. Sci.* **2025**, *44*, 18. [CrossRef]
149. Chen, Y.; Yu, Z.; Han, Z.X.; Sun, W.H.; He, L. A Decision-Making System for Cotton Irrigation Based on Reinforcement Learning Strategy. *Agronomy* **2024**, *14*, 11. [CrossRef]
150. Ben-Gal, A.; Barski, A.; Bukris, O.; Yasuor, H.; O'Shaughnessy, S.A.; Hansen, N.C.; Peeters, A.; Cohen, Y. Dynamic approaches to precision irrigation of cotton. *Precis. Agric.* **2025**, *26*, 64. [CrossRef]
151. Chauhdary, J.N.; Li, H.; Jiang, Y.; Pan, X.W.; Hussain, Z.; Javaid, M.; Rizwan, M. Advances in Sprinkler Irrigation: A Review in the Context of Precision Irrigation for Crop Production. *Agronomy* **2024**, *14*, 47. [CrossRef]
152. Bellvert, J.; Zarco-Tejada, P.J.; Marsal, J.; Girona, J.; González-Dugo, V.; Fereres, E. Vineyard irrigation scheduling based on airborne thermal imagery and water potential thresholds. *Aust. J. Grape Wine Res.* **2016**, *22*, 307–315. [CrossRef]

153. Zhang, C.; Li, X.Y.; Yan, H.F.; Ullah, I.; Zuo, Z.Y.; Li, L.L.; Yu, J.J. Effects of irrigation quantity and biochar on soil physical properties, growth characteristics, yield and quality of greenhouse tomato. *Agric. Water Manag.* **2020**, *241*, 106263. [CrossRef]
154. Ali, A.B.; Elshaikh, N.A.; Hong, L.; Adam, A.B.; Yan, H.F. Conservation tillage as an approach to enhance crops water use efficiency. *Acta Agric. Scand. Sect. B-Soil Plant Sci.* **2017**, *67*, 252–262. [CrossRef]
155. Zhu, X.Y.; Chikangaise, P.; Shi, W.D.; Chen, W.H.; Yuan, S.Q. Review of intelligent sprinkler irrigation technologies for remote autonomous system. *Int. J. Agric. Biol. Eng.* **2018**, *11*, 23–30. [CrossRef]
156. O'Shaughnessy, S.A.; Colaizzi, P.D.; Bednarz, C.W. Sensor feedback system enables automated deficit irrigation scheduling for cotton. *Front. Plant Sci.* **2023**, *14*, 1149424. [CrossRef] [PubMed]
157. Bhatti, S.; Heeren, D.M.; O'Shaughnessy, S.A.; Neale, C.M.U.; LaRue, J.; Melvin, S.; Wilkening, E.; Bai, G. Toward automated irrigation management with integrated crop water stress index and spatial soil water balance. *Precis. Agric.* **2023**, *24*, 2223–2247. [CrossRef]
158. Darko, R.O.; Yuan, S.Q.; Liu, J.P.; Yan, H.F.; Zhu, X.Y. Overview of advances in improving uniformity and water use efficiency of sprinkler irrigation. *Int. J. Agric. Biol. Eng.* **2017**, *10*, 1–15. [CrossRef]
159. Lakhiar, I.A.; Yan, H.F.; Zhang, C.; Wang, G.Q.; He, B.; Hao, B.B.; Han, Y.J.; Wang, B.Y.; Bao, R.X.; Syed, T.N.; et al. A Review of Precision Irrigation Water-Saving Technology under Changing Climate for Enhancing Water Use Efficiency, Crop Yield, and Environmental Footprints. *Agriculture* **2024**, *14*, 1141. [CrossRef]
160. Gao, S.K.; Yu, S.E.; Wang, M.; Meng, J.J.; Tang, S.H.; Ding, J.H.; Li, S.; Miao, Z.M. Effect of Different Controlled Irrigation and Drainage Regimes on Crop Growth and Water Use in Paddy Rice. *Int. J. Agric. Biol.* **2018**, *20*, 486–492. [CrossRef]
161. Rasool, G.; Guo, X.P.; Wang, Z.C.; Ali, M.U.; Chen, S.; Zhang, S.X.; Wu, Q.J.; Ullah, M.S. Coupling fertigation and buried straw layer improves fertilizer use efficiency, fruit yield, and quality of greenhouse tomato. *Agric. Water Manag.* **2020**, *239*, 106239. [CrossRef]
162. Tang, L.D.; Shaikh, I.A.; Tunio, A.; Junejo, A.R.; Hao, L.; Dahri, J.; Mangrio, M.A.; Soothar, R.K.; Khan, Z.A. Effect of Raised Flat Bed and Ridge Planting on Wheat Crop Growth and Yield under Varying Soil Moisture Depletions. *Agronomy* **2024**, *14*, 1404. [CrossRef]

**Disclaimer/Publisher's Note:** The statements, opinions and data contained in all publications are solely those of the individual author(s) and contributor(s) and not of MDPI and/or the editor(s). MDPI and/or the editor(s) disclaim responsibility for any injury to people or property resulting from any ideas, methods, instructions or products referred to in the content.